



Title	Studies on deNO _x Processes for Automotive Vehicles using Ammonia as a Reductant
Author(s)	Saito, Makoto
Citation	大阪大学, 2009, 博士論文
Version Type	VoR
URL	https://hdl.handle.net/11094/27599
rights	
Note	

The University of Osaka Institutional Knowledge Archive : OUKA

<https://ir.library.osaka-u.ac.jp/>

The University of Osaka

**Studies on deNO_x Processes for Automotive
Vehicles using Ammonia as a Reductant**

2009

Makoto Saito

Division of Applied Chemistry
Graduate School of Engineering
Osaka University

Studies on deNO_x Processes for Automotive Vehicles using Ammonia as a Reductant

2009

Makoto Saito

Division of Applied Chemistry
Graduate School of Engineering
Osaka University

Preface

The work of this thesis has been carried out under the guidance of Professor Ken-ichi Machida at the Center for Advanced Science and Innovation, (Division of Applied Chemistry, Graduate School of Engineering, concurrently served), Osaka University, Japan, during 2006-2009.

The purpose of the work in this thesis is to develop the novel deNO_x systems for automobile vehicles assisted by on-board synthesized ammonia from nitrogen and hydrogen or *in situ* produced ammonia related components from NO_x with hydrogen as a reductant.

Makoto Saito

The Center for Advanced Science and Innovation
Osaka University
2-1 Yamadaoka, Suita, Osaka 565-0871, JAPAN

March 2009

Contents

General Introduction	1
-----------------------------------	---

Chapter 1.

Ammonia Synthesis under a Mild Condition Using Hydrogen Permeable Membrane Reactors

1.1. Introduction	4
1.2. Experimental details	5
1.2.1. Gaseous hydrogen-type membrane reactor	5
1.2.2. Water electrolysis-type reactor	8
1.3. Results and discussion.....	9
1.3.1. Ruthenium-loaded catalysts.....	9
1.3.2. Gaseous hydrogen-type membrane reactor	13
1.3.3. Water electrolysis-type reactor	14
1.4. Conclusion.....	16

Chapter 2.

Hydrogen SCR Reaction over Platinum Catalysts Loaded on Trivalent Cations Doped-Tin Pyrophosphates

2.1. Introduction	17
2.2. Experimental details.....	18
2.3. Results and discussion.....	20
2.4. Conclusion.....	26

Chapter 3.

Hydrogen SCR Reaction over Platinum Catalysts Loaded on Sulfated Metal Oxides

3.1. Introduction	28
-------------------------	----

3.2. Experimental details	28
3.3. Results and discussion.....	29
3.3.1. Pt/s-ZrO ₂ catalysts.....	29
3.3.2. Pt/s-CeO ₂ catalysts.....	33
3.3.3. Pt/s-MO _x catalysts (M = Al, Ti, Si, and Sn).....	35
3.4. Conclusion.....	37
Summary	39
References and Notes	41
List of Publications.....	45
Acknowledgment.....	49

General Introduction

Carbon dioxide (CO₂) is the dominant component of greenhouse effect gases as considered as a reason for ascension of global temperature bringing down climate changes and serious hazards [1]. The tolerant temperature rise against pre-industrial levels appears to be at most 2 °C. In order to achieve the 2 °C target, the concentration of such greenhouse gases should be suppressed below 400 ppm of CO₂ equivalent. For this suppression, the developed countries have to cut their emissions by as much as 80% by the middle of 21st century, and the Kyoto Protocol has been adapted for the first step [2].

Japanese goal of the commitment for the Kyoto Protocol is to suppress the greenhouse gas emission below 1.19 billions tons by 2012, but the domestic emission in 2006 has been still 1.34 billions tons. Although the emission from industry category have been already reduced 4.6% against the baseline of 1990's value, the consumer and transportation categories have been discharging, 30% and 16.7% more greenhouse gases than the baseline, respectively [3].

Diesel vehicles have about 25% better well to wheel efficiency than gasoline ones because of their good thermal efficiency and low environmental load for the purification of diesel oils. Japanese government estimates that 1-3 millions tons of CO₂ emission can be decreased in 2015 by replacing gasoline passenger cars to diesel ones. Thus, spread of highly efficient diesel vehicles should be an approach for reducing CO₂ emission, in other words, building low-carbon economics.

Diesel engines achieve high fuel mileage by combusting at lean-burn conditions, however, the excess oxygen concentration in exhaust gases prevents the purification of NO_x to N₂ using the conventional Pt-Rh based three-way catalysts. So that, the detoxification for diesel exhaust gases is performed by following three steps: the oxidation of excess hydrocarbons and carbon monoxide, trapping of particulate matters (PM) consisting of soot and soluble organic fractions, and the reduction of NO_x. Selective catalytic reduction (SCR) of NO_x using various reducing agents such as hydrocarbons, carbon monoxide, and ammonia (or urea as an

ammonia source) have been widely examined for diesel exhaust gases and some of them have been already practiced. For example, Nissan Diesel Motor Co., Ltd. has employed the urea-SCR system for the deNO_x of heavy-duty commercial vehicles and Toyota Motor Corporation has launched the NSR (NO_x Storage Reduction catalysts) system. For the former system ammonia is produced by the hydrolysis of urea and served to reduce NO_x over zeolite-based catalysts *via* the NH₃-SCR reaction [4-6], and the latter one can remove NO_x on the basis of the following two steps; the storage of NO_x in the form of nitrate or nitrite on alkali earth components and then the reduction of stored NO_x with a rich spike containing excess fuels as reductants [7-10]. Although these two methods have enabled to comply with the strict control of diesel emission, they have some respective demerits. The urea-SCR system needs regularly refill of urea water, but their infrastructure is not enough for the demand with passenger cars at the present time. The NSR system deteriorates the mileage since it uses some portion of fuel as a reductant for NO_x.

In this study, the author has focused attention on hydrogen as a suitable candidate for NO_x reduction of vehicles, particularly, passenger cars. Hydrogen is easily prepared by an on-board WGS (water gas shift) reformer from carbon monoxide in the exhaust gas. Hydrogen itself is not only a useful reductant but also a raw substance of ammonia which is suitable reduction agent for NO_x. This thesis deals with the NO_x reduction system involving ammonia synthesis and H₂-SCR reaction *via* the formation of ammonia (ammonium) intermediates.

In **Chapter 1**, novel ammonia syntheses at low reaction temperature were performed using hydrogen permeable membrane reactors. It is well known ammonia can effectively reduce NO_x over vanadium oxide based catalyst [11] or zeolite catalyst [4] with low N₂O emission. Since ammonia itself is a poisonous gas, ammonia needs to be prepared on moving vehicles to perform the NH₃-SCR for NO_x. Ammonia synthesis from nitrogen and hydrogen gases is generally carried out on the high reaction pressure ranging 150-300 atm [12], while the on-board ammonia synthesizer should be operated below 10 atm due to the domestic high pressure gas control law. Ruthenium-based catalysts have been reported as suitable candidate

for ammonia synthesis at low pressure below 10 atm [13,14]. These Ru catalysts have strong affinity to the adsorbed hydrogen which prevents ammonia formation under the high hydrogen partial pressure, so-called “hydrogen poisoning”. The hydrogen permeable membrane can serve atomic hydrogen which has high reactivity toward nitrogen molecules adsorbed on ruthenium active sites to form ammonia, due to the suppression of hydrogen poisoning for Ru catalysts. In **Chapters 2** and **3**, the H₂-SCR of NO_x over platinum loaded catalysts was studied. In particular, **Chapter 2** focused trivalent cations doped tin pyrophosphates, novel proton conductors [15], as a candidate for supporting material. Platinum catalysts loaded on them have possessed excellent deNO_x property under a condition of 5 vol.% of oxygen concentration [16]. The outlet gases from these catalysts were proved to contain some portion of ammonia by our additional tests. Further studies were carried out with focusing ammonium reaction intermediate species. In **Chapter 3**, the other supporting materials were explored from the viewpoint of their solid acidity, and sulfation treatments for metal oxides were performed to possess high solid acidity. The formation mechanism of acid sites and reaction intermediate species were studied using *in situ* diffusion reflection infrared Fourier transform spectra (DRIFTs). Various metal oxides (basic, neutral, and acidic ones) were sulfated to estimate the correlation between their acidity-basicity and accelerative effect for deNO_x properties.

Ammonia Synthesis under a Mild Condition Using Hydrogen Permeable Membrane Reactors

1.1. Introduction

Traditional ammonia synthesis have been carried out using doubly promoted $\text{Fe}_3\text{O}_4\text{-Al}_2\text{O}_3\text{-K}_2\text{O}$ catalysts at high reaction pressure and temperature ranging 150-300 atm and 400-600 °C, respectively [12] to dissociate stable triple bond of nitrogen molecule (bond dissociation energy at 298 K; $\Delta H_{f_{298}} = 945 \text{ kJ}\cdot\text{mol}^{-1}$ [17]). The milder reactions, especially in pressure, are favored to perform the on-board ammonia synthesis for the regulation about high pressure gases. In the last few decades, the Ru-based second generation ammonia synthesis catalysts have been examined to produce ammonia at the lower reaction pressure than 10 atm [13,14]. The catalytic activity for these ruthenium catalysts strongly depend on their supporting materials, in other words, the metal-support interaction is an important factor for ammonia synthesis characteristics. Hence many support materials and promoter have been studied for ruthenium catalysts [13,14,18], and the basic oxides or rare earth oxides ,especially cerium oxide, have been found to be able to possess high catalytic properties for ammonia synthesis [14]. However, such Ru-based catalysts essentially have a strong hydrogen poisoning problem for ammonia synthesis because of considerably high affinity between ruthenium metal and adsorbed hydrogen [18b].

On the other hand, we have reported that the atomic hydrogen released from Ag-Pd hydrogen permeable membrane has high reactivity to suppress the hydrogen poisoning and accelerate the ammonia synthesis over the loaded ruthenium catalysts even under atmospheric pressure [19]. The activation energy of Ru/ Al_2O_3 catalysts for ammonia synthesis were reduced from $66.8 \text{ kJ}\cdot\text{mol}^{-1}$ on the conventional flow-type reactor to $33.1 \text{ kJ}\cdot\text{mol}^{-1}$ on the Ru/ Al_2O_3

catalyst on Ag-Pd membrane reactor,

In this chapter, two types of hydrogen permeable membrane reactors supplying hydrogen in gaseous form or from water electrolysis were examined. Both reactors can supply highly reactive atomic hydrogen through a Pd based alloy membrane. The former one provides the atomic hydrogen by differential partial pressure of hydrogen between two separated chambers and the latter one gives it by electrolysis of water. The ammonia production characteristics were studied by concerning about improvement of ruthenium catalysts, suppression of hydrogen poisoning, and *in situ* hydrogen production.

1.2. Experimental details

1.2.1. Gaseous hydrogen-type membrane reactor

Preparation and catalytic reactions of ruthenium loaded catalysts

The ruthenium catalysts loaded on MgO or MgO-CeO₂ nanocomposite supporting materials were prepared in the following procedure. Firstly, the corresponding metal hydroxide gels were obtained from 0.1 M of their acetate salt aqueous solutions by precipitation method with 3 M ammonia solution. The resultant gels were gathered by a centrifugation and washed with distilled water until no ammonia was detected, and then finally washed with tetrahydrofuran for additional three times. Five percent of ruthenium was loaded by an impregnation method using a transparent orange-colored Ru₃(CO)₁₂ THF solution and moist gels for 12 h in the dark with stirring. The orange solution turned to colorless one after 12 h during the impregnation, which suggests whole of the ruthenium component was completely adsorbed onto hydrogels. Excess solvents were removed with a rotary evaporator, and then the resultant powders were heated at 450 °C for 2 h under a vacuum condition to obtain Ru loaded catalysts. Other Ru catalysts varying the ruthenium source or impregnating method were prepared as comparative examples.

Ammonia synthesis reactions were performed on 0.2 g of each catalyst using a

conventional fixed-bed reactor (inner diameter is about 7 mm) in a temperature range from 300 to 400 °C. A stream of reaction gas (N₂:H₂ = 1:3, both purity are > 99.999%) was fed with a flow rate of 60 mL·min⁻¹ and the outlet gas was introduced into a dilute sulfuric acid to absorb the formed ammonia. The formation rate was calculated with the change of the pH value of the absorber using the following equation:

$$r = \frac{(10^{\text{pH}_{t=0}} - 10^{\text{pH}_{t=t}})V}{t \cdot m} \quad (\text{Eq. 1-1})$$

where, r is the formation rate, t is the reaction time, V represents the volume of sulfuric acid, and m is the weight of catalyst.

Fabrication and catalytic test of the membrane reactor

Catalyst precursor powders, a ruthenium impregnated MgO-CeO₂ composite gel, Ru(CO) _{n} /[Mg(OH)₂-Ce(OH) _{x}] ($x = 3\sim 4$) was dispersed in ethanol and spread on a Ag-Pd alloy membrane (Pd: 75 at.%, reaction area: 9 cm²) and dried overnight (specific catalyst loading amount was about 3 mg·cm²). It was subsequently heated at 450 °C in a hydrogen stream to obtain the ruthenium catalyst loaded membrane and fabricate the membrane reactor illustrated in Fig. 1-1.

Ammonia synthesis reactions were performed by flowing nitrogen gas to the catalyst-loaded side of membrane and various composition of nitrogen-hydrogen mixture to the opposite (metal-exposed side) in a flow rate of 40 mL·min⁻¹ to control a hydrogen permeation rate. The permeation rate for hydrogen was determined using a gas chromatograph (GC-8A, Shimadzu) equipped with a molecular sieve 5A filled column. The optimum composition of nitrogen-hydrogen mixed gas was fed to the both sides to evaluate the catalytic performance for ammonia synthesis as a conventional flow-type reactor. Ammonia formation rate was determined using the absorbing method described above.

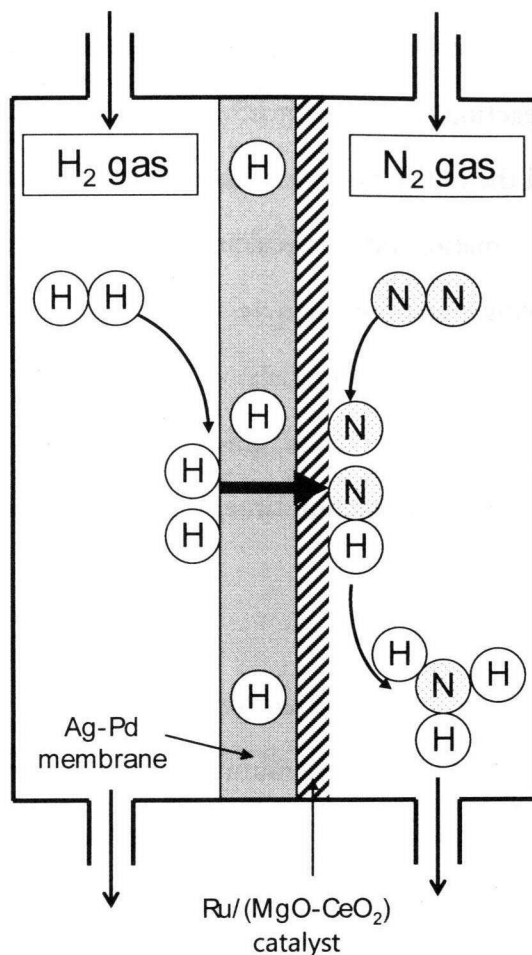


Figure 1-1. A schematic illustration of the gaseous type hydrogen permeable membrane reactor.

Characterization of catalysts

The hydrogen chemisorption measurements were performed by using a thermal conductivity detector (TCD) attached to the gas chromatograph according to the conventional pulse technique [20]. To reduce Ru metal particles and eliminate adsorbed species completely, all samples were pretreated in hydrogen flow at 450 °C for 2 h, and then degassed in an Ar flow at 450 °C for 2 h before starting the above pulse experiments. The metal dispersion and size of ruthenium metal particles were calculated from results of hydrogen chemisorption experiments as dissociated molecular hydrogen adsorbing on spherical metal particle ($H_{ads}/Ru = 1$) [21]. The hydrogen consumption profiles were also observed by temperature-programmed reduction (TPR) experiments to estimate the reduction behavior of catalysts using a TCD. The H_2 -TPR measurements were carried out with a heating rate of 5

$^{\circ}\text{C}\cdot\text{min}^{-1}$ under a hydrogen stream on the catalysts pre-oxidized at $550\text{ }^{\circ}\text{C}$ for 2 h in air. The specific surface area values were measured using Brunauer-Emmett-Teller's (BET) method (Flow Sorb 2300II, Micrometrics). The microstructures of the catalysts were observed using a transmission electron microscope (JEM-2010F, JEOL) equipped with energy dispersive X-ray (EDX) unit (resolution $\approx 1.1\text{ nm}$). The valence state for cerium was analyzed by using an X-ray photoelectron spectrometer (XPS) (AXIS-165, Shimadzu).

1.2.2. Water electrolysis-type reactor

Fabrication and catalytic reaction of a membrane reactor

Preparation of ruthenium metal catalyst on the outer side of hydrogen permeable membrane tubes were prepared by an electrodeposition method using one-sided shielding Ag-Pd alloy tubes as a cathode, a platinum wire as an anode, and a $0.1\text{ M RuCl}_3\text{-ZnCl}_2$ aqueous solution as an electrolyte. The deposited zinc components were removed with a dilute hydrochloric acid, then the resultant Ru-electrodeposited tubes were washed with aqueous ammonia and distilled water to remove chlorine residues. The resultant Ru/Ag-Pd tube (reaction area: ca. 7 cm^2 , outer diameter: 5 mm , thickness: $100\text{ }\mu\text{m}$) was dipped in a dilute aluminum *sec*-butoxide solution and dried for 12 h in the air to coat with a thin porous alumina layer.

The schematic illustration of water electrolysis-type hydrogen permeable membrane reactors using above mentioned Ru/Ag-Pd tube is shown in Fig. 1-2. 6 M of dense sodium hydroxide aqueous solution as an electrolyte and a platinum as a counter electrode were put in inner side of the Ru/Ag-Pd reaction tube as a working electrode and 20 mA of constant electric current was charged to produce hydrogen. Ammonia synthesis was carried out by flowing $50\text{ mL}\cdot\text{min}^{-1}$ to the outer side of the reaction tube at $100\text{ }^{\circ}\text{C}$. The ammonia formation rate was determined by the same method described above.

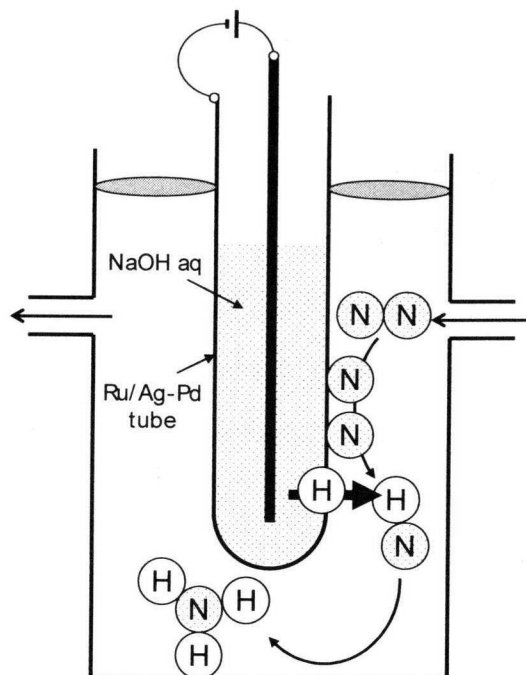


Figure 1-2. A schematic illustration of the water electrolysis type hydrogen permeable membrane reactor.

1.3. Results and discussion

1.3.1. Ruthenium-loaded catalysts

Figure 1-3 shows ammonia formation rate values over ruthenium catalysts loaded on magnesia support with different precursors at 300-400 °C. Ammonia was hardly synthesized over the Ru/MgO catalyst prepared from ruthenium chloride due to poisoning of residual chlorine [14]. Other two ruthenium catalysts derived from ruthenium carbonyl complex as ruthenium source produced ammonia at atmospheric pressure, and especially the moist-gel impregnated catalyst generated about

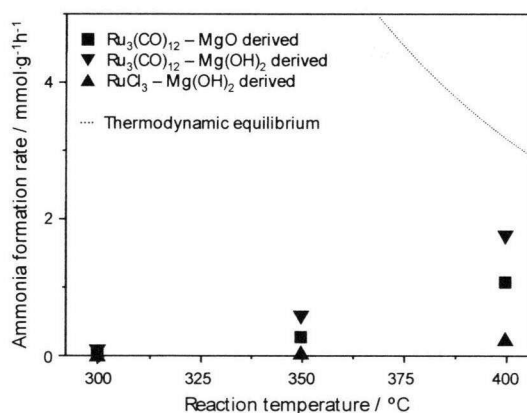


Figure 1-3. Temperature dependencies of ammonia formation rate on Ru/MgO catalysts prepared from Ru₃(CO)₁₂ complex and calcined MgO powder (filled square), Ru₃(CO)₁₂ complex and wet Mg(OH)₂ gel (filled upturned triangle), RuCl₃ and wet Mg(OH)₂ gel (filled downturned square).

twice amount of ammonia compared with the catalyst prepared from the calcined MgO support. The specific BET surface area of the catalyst prepared from moist-gels was 190 m²·g⁻¹

and that prepared from the calcined powder was $116 \text{ m}^2 \cdot \text{g}^{-1}$. This difference should be responsible for the enhancement of catalytic performance for ammonia synthesis. A nitrogen adsorption isotherm of Ru/MgO catalyst prepared from moist-gel impregnating was classified as type IV of IUPAC category, suggesting the existence of mesopore. The pore radius calculated by Dollimore-Heal equation [22] using adsorption isotherm ranges from 1-9 nm (Fig. 1-4) and the

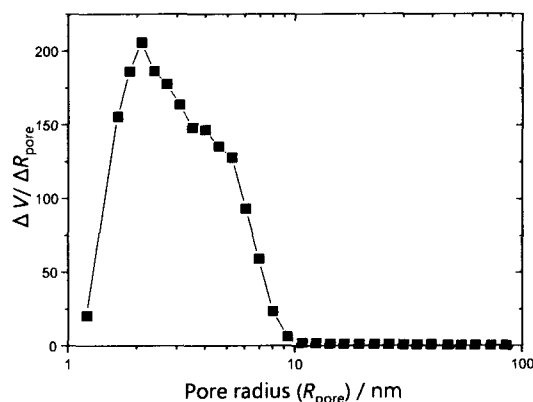


Figure 1-4. A pore radius distribution calculated by D-H method on the desorption isotherm of Ru/MgO catalyst prepared by moist-gel impregnation method.

total mesopore volume was $0.65 \text{ mL} \cdot \text{g}^{-1}$. This mesopore is responsible for the high surface area. The formation of such mesoporous structure owes to the simultaneous decarbonylation of ruthenium carbonyl complex during the dehydration of magnesium hydroxide. Nucleophilic attack of hydroxyl group of magnesium hydroxide gel toward carbonyl group of ruthenium carbonyl has been reported by D'Orenelas et al [23]. It suggests that both hydroxide gels and carbonyl complex forms the well dispersed network structure illustrated in Fig. 1-5. Mass analysis for the discharged gas was carried out during heating treatment of catalyst precursor.

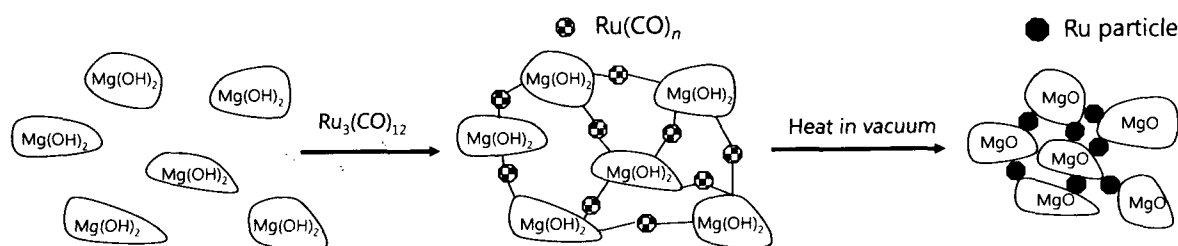


Figure 1-5. Plausible mechanism for the formation of microstructure of Ru/MgO catalyst.

Temperature programmed reaction profiles recorded for $m/z = 2$ (H_2), 18 (H_2O), 28 (CO), and 44 (CO_2) are shown in Fig. 1-6. Various gases including H_2O and CO were generated by the dehydration reaction of magnesium hydroxide and the decomposition of ruthenium carbonyl complex, respectively, and a part of CO and H_2O produced H_2 and CO_2 via a water-gas shift

reaction ($\text{CO} + \text{H}_2\text{O} \rightarrow \text{CO}_2 + \text{H}_2$) catalyzed by ruthenium metal over 150 °C. These gases prevent MgO particles from crystal growth during the calcination, and as a result the mesoporous structure with high surface area was formed.

Ammonia formation rate over ruthenium catalysts on various compositions of MgO-CeO₂ composite (Mg:Ce = 100:0, 75:25, 50:50, 25:75, and 0:100) are shown in Fig. 1-7 and Table 1-1. The reaction rate and turn over frequency (TOF) value increased by hybridizing MgO and CeO₂ support materials and the optimum ratio was found to be 50:50. The reaction rate of the optimum composition of Ru/(MgO-CeO₂) catalyst reached to a thermodynamic equilibrium state, namely, the ammonia formation rate above 375 °C was theoretically suppressed.

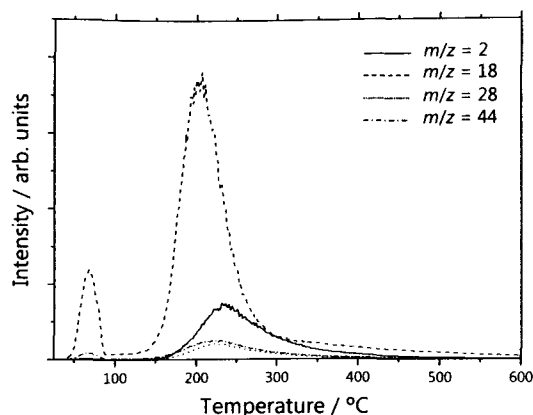


Figure 1-6. TPR-mass profile for catalyst precursor by moist-gel impregnation method in vacuum. Respective $m/z = 2, 18, 28,$ and 44 correspond to $\text{H}_2, \text{H}_2\text{O}, \text{CO},$ and CO_2 .

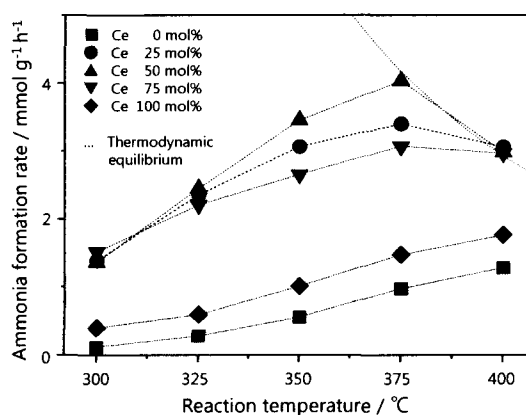


Figure 1-7. Temperature dependencies of ammonia formation rate on various compositions of Ru/(MgO-CeO₂) catalysts

Table 1-1. BET surface area, ruthenium particle size, and turn-over frequencies of Ru/(MgO-CeO₂) catalysts

MgO:CeO ₂ (molar ratio)	BET surface area [m ² ·g ⁻¹]	TOF at 325 °C [s ⁻¹]
0:100 (CeO ₂)	121.8	3.4×10^{-3}
25:75	157.6	6.3×10^{-3}
50:50	144.8	8.0×10^{-3}
75:25	142.3	4.9×10^{-3}
100:0 (MgO)	200.3	1.8×10^{-3}

XRD patterns of various compositions of Ru/(MgO-CeO₂) catalysts are shown in Fig. 1-8. The peak intensity attributed to MgO in the XRD patterns weakened with increase of CeO₂ content and finally such peaks were disappeared at the CeO₂ content more than 50 mol%. Both of them are known to form no solid solutions [24] and the MgO peaks appeared after heating in air at 600 °C. These results suggest that the MgO component is in amorphous or fine particle state which suppresses crystal growth of CeO₂ during heat treatment.

The H₂-TPR profiles shown in Fig. 1-9 represent the reduction behavior of the surface ceria component. The reduction temperatures of respective CeO₂ and Ru/CeO₂ samples were 520 and 400 °C. While, the reduction on Ru/(MgO-CeO₂) apparently took place at low temperature (280 °C). Precious metals such as Pt and Rh have reported to enhance the reduction property of ceria component by so called SMSI (strong metal-support interaction) effect [25]. As shown in the TEM micrograph (Fig. 1-10), ruthenium metal particles were well dispersed and closely interacted with the support material, resulting in acceleration of the ceria reduction. Partially reduced ceria, CeO_{2,δ}, is known to be an

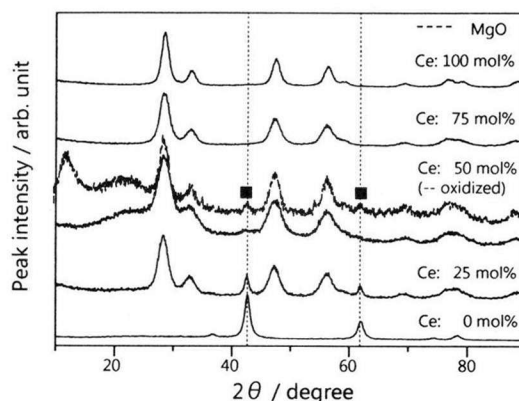


Figure 1-8. XRD profiles of Ru/(MgO-CeO₂) (CeO₂: 0, 25, 50, 75, and 100 mol%) catalysts as prepared. Dashed line indicates an oxidized Ru/(MgO-CeO₂) catalyst (CeO₂: 50 mol%) at 600 °C in air.

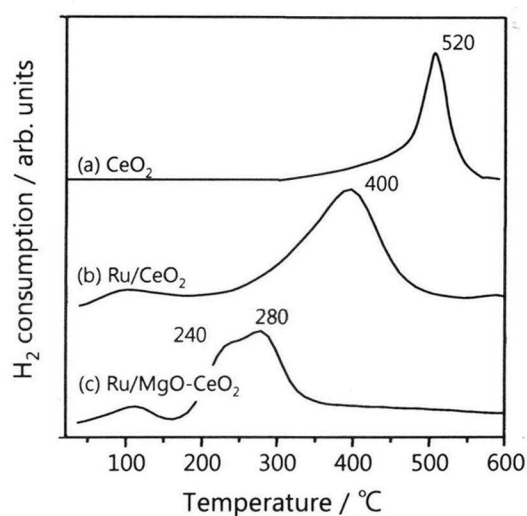


Figure 1-9. Hydrogen TPR profiles of (a) sole CeO₂ [25], Ru/CeO₂, and (c) Ru/(MgO-CeO₂) (CeO₂: 50 mol%).

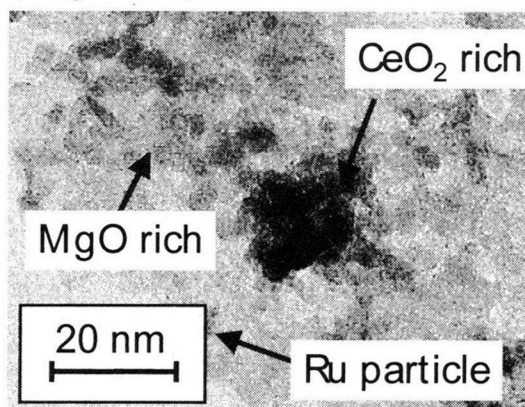
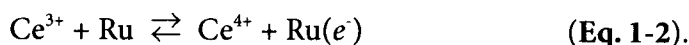


Figure 1-10. A TEM image of Ru/(MgO-CeO₂) catalyst, magnification was 1.5×10^6 .

n-type semiconductor [26] and mobile electrons in CeO_{2.6} can be donated to Ru metal particles, leading to promotion the cleavage of N≡N triple bond as following scheme [27];



Compositing of magnesia and ceria in nanometer scale increased its surface area and electrodonation ability of the partially reduced ceria. The ammonia synthesis was accelerated by the above two effects.

1.3.2. Gaseous hydrogen-type membrane reactor

Figure 1-11 shows the dependence of the ammonia formation rate with the gaseous hydrogen type hydrogen permeation rate on the membrane reactor at atmospheric pressure in the temperature range of 300-400 °C. The results on the conventional flow-type reactor (using molecular hydrogen) are also shown by dashed lines as references. The ammonia formation rate on the membrane reactor increased with the hydrogen permeation rate below the optimum value at each temperature. The optimal values

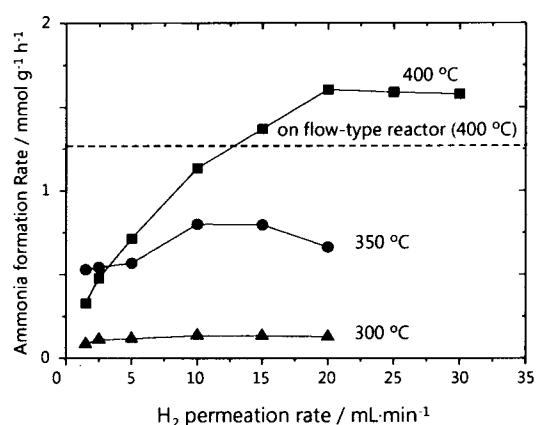


Figure 1-11. Hydrogen permeation rate dependences for ammonia formation rate over the Ru/(MgO-CeO₂) (CeO₂: 50 mol%) catalyst on the hydrogen permeable membrane at 300-400 °C, in a 40 mL.min⁻¹ of a nitrogen stream. Dotted line indicates the formation rates for the flow-type reactor, obtained by flowing 20 mL.min⁻¹ of hydrogen and 40 mL.min⁻¹ of nitrogen mixed gas at 400 °C.

were 10 mL.min⁻¹ at 300 and 350 °C and 20 mL.min⁻¹ at 400 °C. On the other hand, the ammonia formation rate decreased by supplying the excess amount of hydrogen. The excess hydrogen negatively affect to the ammonia formation (so-called hydrogen poisoning) [19], once partial pressure for hydrogen becomes greater than their threshold value. The ammonia formation rate on the membrane reactor at 400 °C was 1.6 mmol.g⁻¹.h⁻¹, which was higher than the result on the flow-type reactor (1.3 mmol.g⁻¹.h⁻¹). The reaction order for partial pressure of hydrogen (P_{H_2}) on the membrane reactor was 0.71, which was higher than that of the conventional flow-type one (0.59). These

results are responsible for the highly reactive atomic hydrogen supplied through the Ag-Pd membrane, which spilled over to the ruthenium metal particle to react with the dissociated nitrogen atoms.

The ammonia formation was accelerated considerably when increasing the reaction pressure to 0.6 MPa. Figure 1-11 shows variation of the ammonia formation rate obtained with various amounts of hydrogen fed to the membrane reactor at 400 °C. The maximum ammonia formation rate (ca. 7.5 mmol·g⁻¹·h⁻¹) was observed with a hydrogen permeation rate of 12.5 mL·min⁻¹, which was about twice higher than that of the flow-type reactor (ca. 4.5 mmol·g⁻¹·h⁻¹) under the same N₂-H₂ composition. A stronger acceleration for ammonia synthesis was attained by supplying atomic hydrogen compared to hydrogen that supplied by a conventional way under high reaction gas pressure. This result supports that effective ammonia production is realized on the present membrane reactor. For a conventional flow-type reactor, hydrogen and nitrogen gases tend to adsorb and dissociate simultaneously at the active site of the catalyst. Consequently, these reactions proceed competitively, and the catalysts are poisoned by hydrogen having high affinity. On the other hand, atomic hydrogen was supplied through the Ag-Pd membrane and reacted with dissociated atomic nitrogen on the ruthenium catalyst attached to such a hydrogen-permeable membrane. Consequently, the Ru metal dissociates nitrogen molecules and the resultant atomic nitrogen reacts quickly with the supplied hydrogen atoms to form ammonia. Therefore, hydrogen poisoning can be avoided in the membrane reactor by changing the hydrogen supply manner.

1.3.3. Water electrolysis-type reactor

Figure 1-12 shows the total ammonia

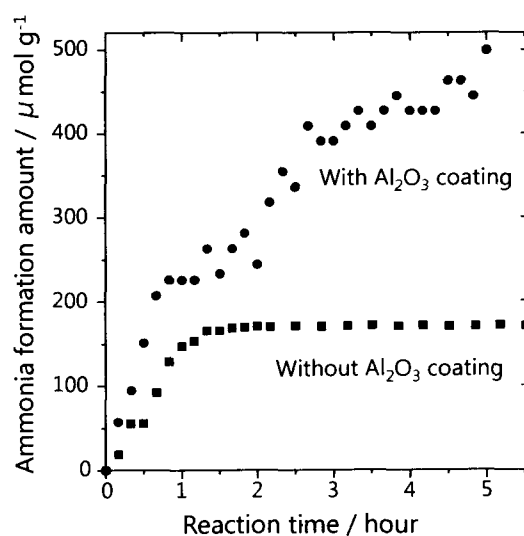


Figure 1-12. Total ammonia production amount with reaction time over the ruthenium metal catalysts coated with alumina layer (filled circle) and uncoated (filled square) on the electrolysis type membrane reactor.

formation amount over the ruthenium catalyst on the water-electrolysis type membrane reactor at 100 °C. Both catalysts could produce ammonia even at the considerably low reaction temperature of 100 °C. Only a few studies have succeeded ammonia synthesis at this temperature. The hydrogen conversion to ammonia on this reactor was about 0.1 %. The barium oxide doped ruthenium catalyst on activate carbon (BaO-Ru/A.C.) have been reported to attain the best catalytic performance for ammonia synthesis [18i] and its conversion is about 0.01% at 315 °C. Compared with such catalysts, these electrodeposited metal catalysts directly contact with hydrogen permeable membrane, so that the atomic hydrogen supplied from the membrane can easily spill over to ruthenium active site to produce ammonia. On the uncoated catalyst, however, ammonia formation ceased irreversibly within about 1-2 hours, while alumina coated catalyst linearly synthesized ammonia for at least 8 hours.

The SEM observation (see Fig. 1-13) revealed that the surface morphology of uncoated catalyst drastically changed through the ammonia synthesis. The porous structure observed before the reaction was disappeared after the reaction and they aggregated to large particles because of exothermic reaction for ammonia formation. On the contrary, the alumina coated catalyst kept the microporous structure and no deactivation in catalytic performance was observed. The coated alumina layers should suppress the aggregation of ruthenium metal particles.

It is well known that catalytic activity of ruthenium based catalysts is considerably enhanced by addition of promoters having

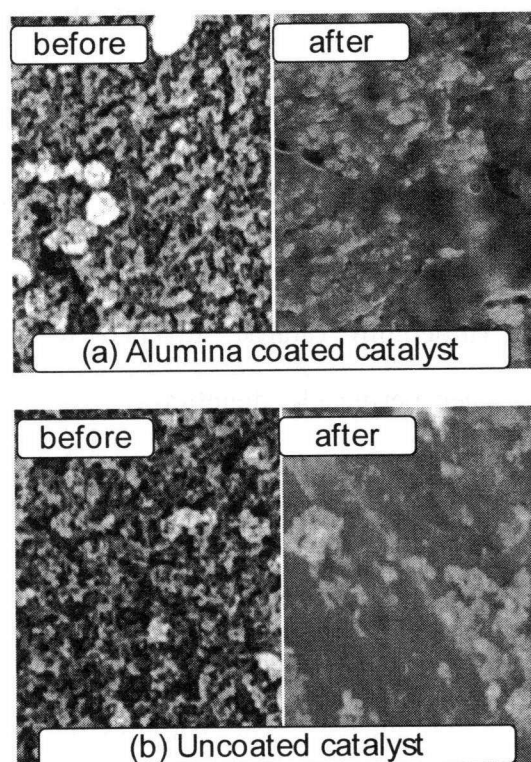


Figure 1-13. Surface morphology change of ruthenium catalysts on Ag-Pd tube before (left) and after (right) ammonia synthesis reaction with (a) alumina coating and (b) no alumina coating.

electron donation ability such as alkali earth [13]. The ruthenium catalyst of this reactor closely attached to the Ag-Pd tube as an anode, thus a negative charge may promote the catalytic property like an electrochemical promotion [28].

1.4. Conclusion

Ammonia formation activity of ruthenium catalysts was enhanced by supplying the atomic hydrogen from Ag-Pd hydrogen permeable membrane reactor because of the suppression of hydrogen poisoning of ruthenium catalyst and high reactivity of atomic hydrogen. The gaseous type membrane reactor achieved about 1.5-2 times of ammonia formation activity as much as the conventional flow type reaction at high-pressure condition (0.6 MPa) due to the above mentioned effect. The water electrolysis type membrane reactor produced ammonia even at low temperature about 100 °C. The electrodeposited ruthenium metal catalysts on the membrane should be activated by electron donation from the Ag-Pd anode, and their deactivation caused by sintering with ammonia formation heat was effectively suppressed by coating with a thin alumina layer.

Hydrogen SCR Reaction over Platinum Catalysts Loaded on Trivalent Cations Doped-Tin Pyrophosphates

2.1. Introduction

The selective catalytic reduction of nitrogen oxides (NO_x: NO and NO₂) using hydrogen as a reductant (H₂-SCR) is a potent candidate for removing method of NO_x from diesel exhaust gases containing excess oxygen (ca. 10 vol.%). The SCR reaction with hydrogen progresses even at lower operation temperature of about 70 °C, while other reducing agents such as hydrocarbons [29,30], carbon monoxide [31], and ammonia (or urea as an ammonia source) [32-34] reduce NO_x at above 150 °C, and the direct decomposition of NO_x (2NO → N₂ + O₂; 2NO₂ → N₂ + 2O₂) requires at least 500 °C [35,36]. The low operation temperature of H₂-SCR is preferred to the deNO_x for passenger diesel vehicles, because of low temperature of exhaust gas (< 150 °C) in the city driving mode. Furthermore, hydrogen is a harmless and clean reductant compared with above mentioned reducing agents. Although the H₂-SCR can remove NO_x in high conversion, much nitrous oxide (N₂O), which is one of the greenhouse effect gases having about 300 times baleful influence as much as carbon dioxide, tends to be formed as a byproduct.

Recently some studies on H₂-SCR reactions have found that ammonium intermediate species are formed over some platinum loaded catalysts and deNO_x reaction progresses *via* NH₃-SCR scheme using them [37,38]. In addition, an excellent deNO_x performance at 5 vol.% of oxygen concentration has been reported over the platinum catalyst loaded on a novel proton conductor, trivalent cation doped tin pyrophosphates (Sn,M)P₂O₇ (M = In, Al, etc.) [16]. They have proposed that H₂ molecular dissociated to protons and electrons, forming a local anodic site, and NO_x reacted with protons and electrons at a local cathodic site to form N₂ and

H₂O. As a result, an electrochemical local cell was formed at platinum islands on proton conductive powders (Fig. 2-1). Our retesting have confirmed, however, that above good

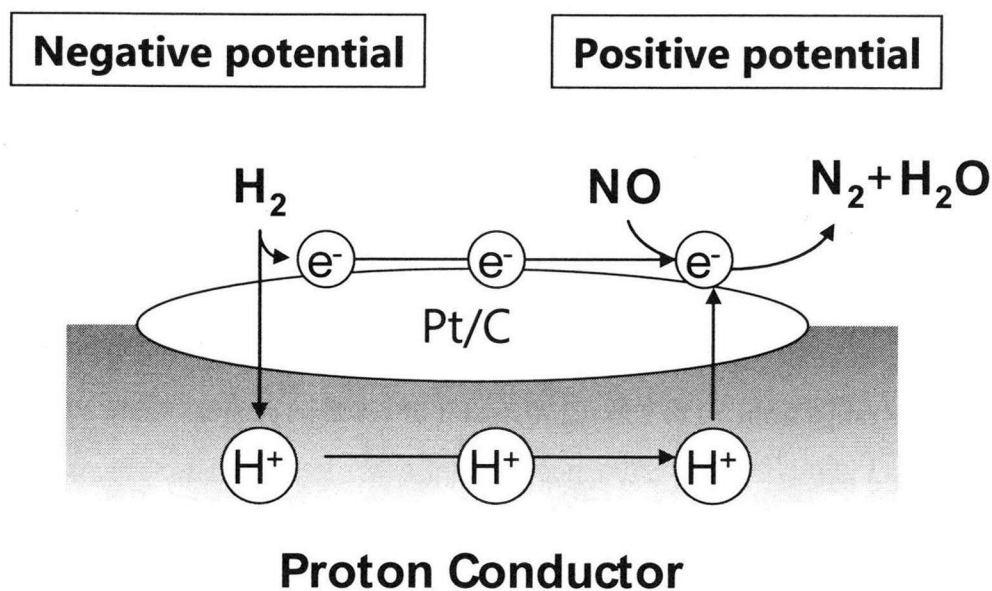


Figure 2-1. Schematic illustration of H₂-SCR mechanism over Pt/(Sn,In)P₂O₇ catalyst [16].

catalytic performance for deNO_x sharply disappeared by increasing oxygen concentration up to 10 vol.% as seen in real diesel exhaust gases, and the adsorption of ammonium species were observed by an *in situ* DRIFT (Diffuse Reflectance Infrared Fourier Transform) spectroscopy. This adsorbed ammonium species seems to incorporate deNO_x reaction.

In this chapter, the reaction intermediate species and their origin were studied over Pt/(Sn,M)P₂O₇ (M = In, Fe, Sc) catalysts using an *in situ* DRIFT spectroscopy measurement in order to probe the reaction mechanism on them. NH₃-TPD (temperature programming desorption) studies were also conducted to discuss the factors for deNO_x catalytic activity from the viewpoint of their solid acidity.

2.2. Experimental details

Preparation and catalytic reaction of platinum catalysts

Tin pyrophosphate powders substituted by trivalent ions, (Sn_{0.9}M_{0.1})P₂O₇ (M = Fe, In, or Sc), were prepared by a conventional solid state reaction. Reagent grade (NH₄)₂HPO₄, SnO₂

and 10 mol% of M_2O_3 ($M = Fe, In, \text{ or } Sc$) were well ground and calcined twice in an alumina crucible at 327 °C and 650 °C for 2.5 h in air. Then, 1 wt% of platinum was loaded to them by an incipient wetness impregnation method using a $Pt(NO_2)_2(NH_3)_2$ solution, followed by drying at 120 °C overnight and heating at 600 °C for 2 h in air. A platinum catalyst supported on an undoped tin pyrophosphate powder (Pt/SnP_2O_7) was also prepared in the same procedure as a comparison.

Catalytic test reactions were performed on 0.1 g of each $Pt/Sn_{0.9}M_{0.1}P_2O_7$ ($M = Fe, In, \text{ or } Sc$) catalysts using a conventional fixed-bed quartz tube reactor (inner diameter; ca. 7 mm) at the temperature range from 70 to 250 °C. A stream of reaction gas (0.1 vol.% NO, 0.4 vol.% H_2 , 10 vol.% O_2 and balance of N_2) was fed with a flow rate of 50 mL·min⁻¹. The composition for the outlet gas was analyzed using an online FT-IR spectrometer (Perkin-Elmer SPECTRUM 2000 with an MCT detector) with two KBr windows equipped gas cell (optical length; 10 cm). Concentrations of NO, N_2O , and NO_2 were determined using peak areas of their absorbance peaking at 1911, 2212, and 1586 cm⁻¹, respectively. The N_2 yield based on NOx reduction was determined by subtracting concentration of NO, N_2O , NO_2 , and NH_3 in outlet gas from the inlet NO concentration. The NOx (NO and NO_2) conversion and $N_2 + NH_3$ selectivity were determined as follows:

$$\text{NOx conversion (\%)} = \frac{([\text{NO}]_{inlet} - [\text{NO}_x]_{outlet})}{[\text{NO}]_{inlet}} \times 100 \quad (\text{Eq. 2-1})$$

$$\text{N}_2 + \text{NH}_3 \text{ selectivity (\%)} = \frac{(2 \times [\text{N}_2]_{yield} + [\text{NH}_3]_{yield})}{(2 \times [\text{N}_2]_{yield} + [\text{NH}_3]_{yield} + 2 \times [\text{N}_2\text{O}]_{outlet})} \times 100 \quad (\text{Eq. 2-2}).$$

In situ DRIFT spectroscopy

The *in situ* DRIFT spectra were recorded using a FT-IR apparatus with a diffusion reflection cell equipped a ZnSe window. The spectra were collected by accumulating 50 scans at a resolution of 4 cm⁻¹ in the range from 4000 to 800 cm⁻¹. Reference spectra in N_2 flow for each catalyst were recorded at corresponding temperatures and then subtracted from each

spectrum under the reaction gas flow.

Characterization of Catalysts

Amounts of Pt loading and their particle size were checked by an ICP-AES analyzer (SPS4000, SII) and transmission electron microscope (JEM-2010F, JEOL), respectively. The X-ray diffraction measurements for the catalysts were carried out by using an X-ray diffractometer (RINT-2200, Rigaku) with Cu-K α radiation. Ammonia temperature programmed desorption (NH₃-TPD) profiles over each catalysts (0.2 g) were recorded using a quadrupole mass-spectrometer (Prisma Plus QMG220M, Pfeiffer Vacuum). Each catalyst was charged in a quartz tube and pretreated in an oxygen stream (50 mL·min⁻¹) at 500 °C for 1 h and cooled to 100 °C in nitrogen atmosphere. Then ammonia adsorption was carried out by exposing 0.1 MPa of ammonia for 1 h. The TPD experiments were performed in a He stream (30 mL·min⁻¹) from 100 to 700 °C with heating ramp of 10 °C·min⁻¹.

2.3. Results and discussion

Characterization of catalysts

TEM micrograph of platinum catalyst powder (Pt/Sn_{0.9}Fe_{0.1}P₂O₇) is shown in Fig. 2-2. The Pt particle with about 1-5 nm diameter were well dispersed on the support grain about 20-50 nm in diameter. All the other trivalent cation doped samples showed same morphology.

XRD analyses revealed every samples crystallized in cubic SnP₂O₇ phase (PDF #29-1352) and their cell parameters have a good

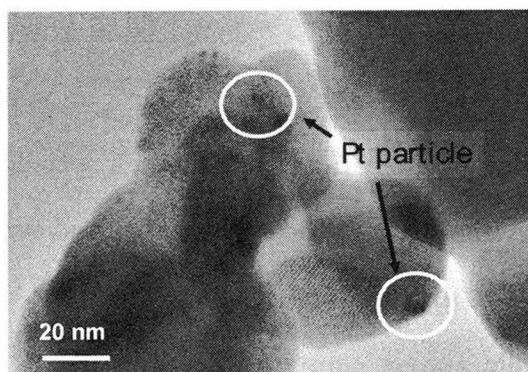


Figure 2-2. A TEM image of Pt/(Sn_{0.9}Fe_{0.1})P₂O₇ catalyst.

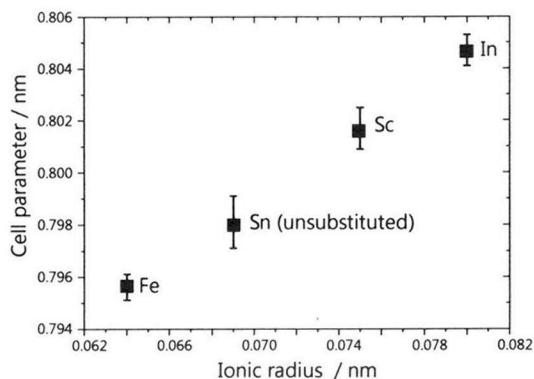


Figure 2-3. Relationship for between ionic radius [39] and cell parameter values for (Sn_{0.9}M_{0.1})P₂O₇ (M = In, Fe, or Sc).

correlation with the ionic radii of doped cations (Fig. 2-3), suggesting the formation of solid solutions. The composition of tin phosphates agreed with the desired ratio ($M:(Sn+M) = 1:10$, $(Sn+M):P = 1:1.98 \pm 0.02$) and no contamination such as Al was detected. The platinum loading was determined 1.01 ± 0.01 wt.%.

Catalytic Activity for H₂-SCR

The NO_x conversion, N₂ selectivity and NO₂ ratio in the residual NO_x over a series of catalysts are shown in Fig. 2-4. The undoped Pt/SnP₂O₇ catalyst exhibited high NO_x reducing property reaching about 80 % at low temperature below 100 °C, however, their N₂ selectivity did not exceed 40 % and much N₂O as a by-product was generated. On the other hands, each trivalent cation doped sample Pt/(Sn_{0.9}M_{0.1})P₂O₇ (M = In, Fe, or Sc) showed high NO_x conversion at the higher reaction temperature above 100 °C with high N₂ + NH₃ selectivity. Especially, Fe³⁺ or Sc³⁺ doped ones achieved about 90% of NO_x conversion. The order for catalytic performance at 140 °C (Sc-doped > Fe-doped > In-doped > undoped) was summarized in Table 2-1 with their specific BET surface area values. There was no relationship between the catalytic performance and surface area. The residual NO_x mainly consisted with NO at the optimum temperature range for the case of the trivalent cation doped catalysts, while almost constant NO ratio about 30-40 % was observed on the undoped catalyst (Pt/SnP₂O₇). These differences such as suitable reaction temperature and residual NO_x compositions suggest that the deNO_x mechanism on the platinum supported tin pyrophosphate catalysts changes by substituting trivalent cations for Sn⁴⁺ site.

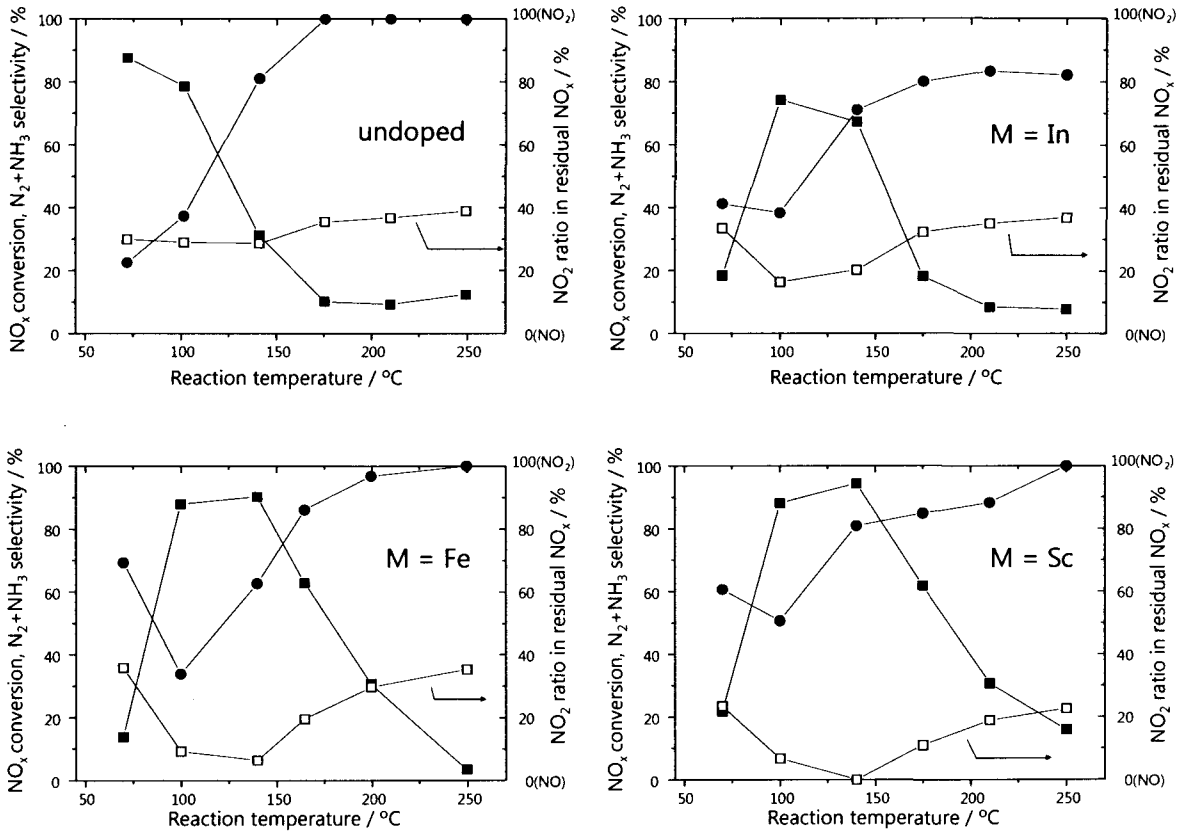


Figure 2-4. Temperature dependences of NO_x conversion (filled square), N₂ + NH₃ selectivity (filled circle), and NO₂ ratio in the residual NO_x (open square) on a series of Pt/(Sn_{0.9}M_{0.1})P₂O₇ catalysts (M = In, Fe, or Sc). Weight of catalysts; 0.1g, gas flow rate; 50 mL·min⁻¹, gas composition; 0.1 vol.% NO, 0.4 vol.% H₂, 10 vol.% O₂, and balance of N₂.

Table 2-1. NO_x removal rate and conversion to N₂(+ NH₃) on a series of (Sn,M)P₂O₇ catalysts at 140 °C and their specific BET surface area

Doped cation	deNO _x rate (conv. to N ₂ + NH ₃) / %	Specific BET surface area/ m ² ·g ⁻¹
undoped	30.3 (24.5)	4.4
In	67.2 (47.8)	3.5
Fe	90.2 (56.4)	4.2
Sc	94.4 (76.4)	3.7

Reaction mechanism for deNO_x reaction

Figure 2-5 shows the *in situ* DRIFT spectra for a series of Pt catalysts at 140 °C. Three broad bands (2900, 3100, and 3250 cm⁻¹), two sharp bands (1358, 1440 cm⁻¹), and a weak band (1620 cm⁻¹) were observed. The broad bands at around 2900-3250 cm⁻¹ are attributed to symmetric and asymmetric N-H stretch vibration of ammonium species on the Brønsted acid sites. The two bands at 1440, and 1620 cm⁻¹ are assigned to adsorbed ammonium species on Brønsted acid sites, and Lewis acid sites, respectively [38]. The peak heights over a series of catalysts are summarized in Table 2-2, together with the NO_x conversion values. The order for amount of the adsorbed ammonium species well agrees with that for the catalytic performance at 140 °C. It implies that the adsorbed ammonium species are responsible for the good deNO_x activity, especially for the high N₂ selectivity.

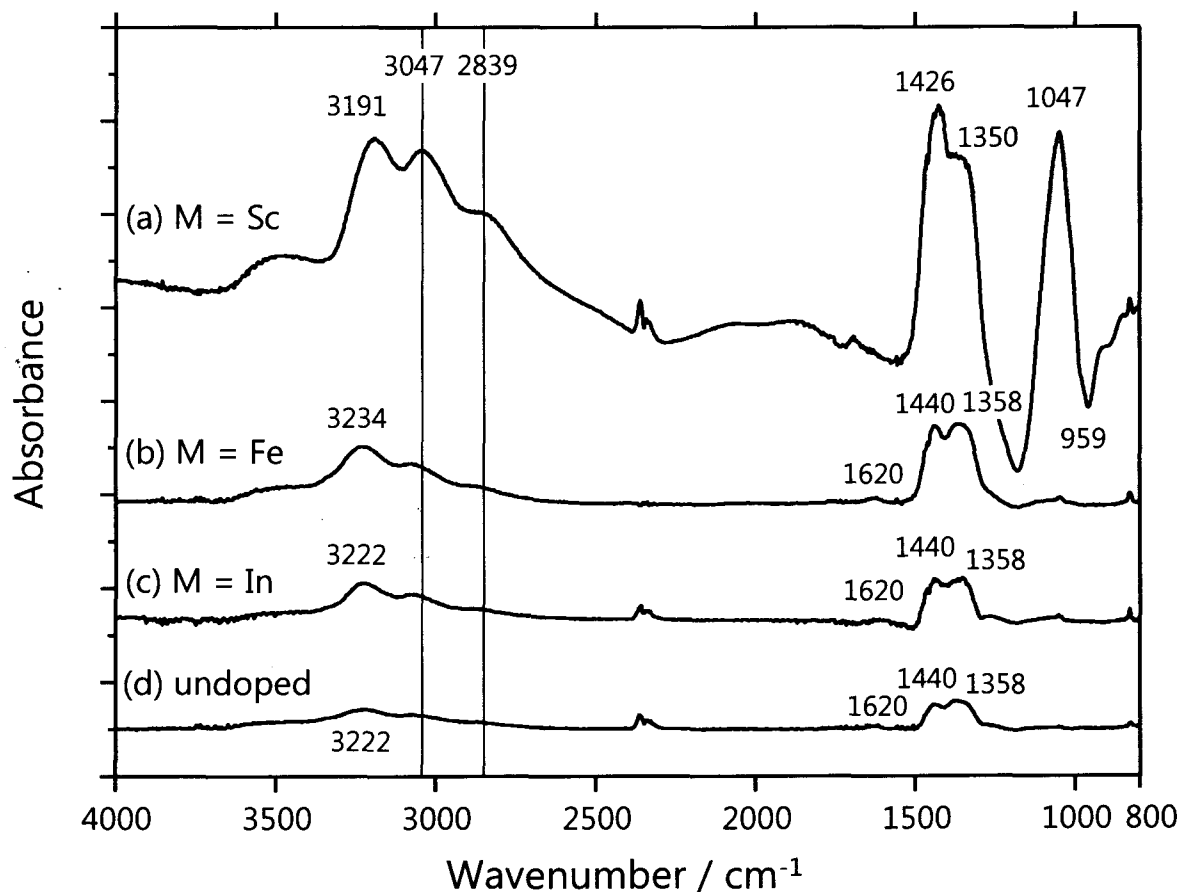


Figure 2-5. *In situ* DRIFT spectra of adsorbed species on Pt/(Sn,M)P₂O₇ catalysts doped with M = Sc (a), Fe (b), In (c), and undoped (d) in the reaction gas flow at 140 °C, pretreatment was done in oxygen atmosphere at 400 °C for 1h.

Table 2-2. NO_x removal rate and conversion to N₂(+ NH₃) on a series of (Sn,M)P₂O₇ catalysts, peak height of absorbance for adsorbed ammonium species, and ammonia adsorb amount over a series of catalysts at 140 °C

Doped cation	deNO _x rate (conv. to N ₂ + NH ₃) / %	Peak height		Adsorbed ammonia / μmol·g ⁻¹
		1440 cm ⁻¹	3220 cm ⁻¹	
undoped	30.3 (24.5)	0.027	0.020	8.4
In	67.2 (47.8)	0.046	0.035	10.4
Fe	90.2 (56.4)	0.087	0.058	14.0
Sc	94.4 (76.4)	0.370	0.210	19.3

Their ammonia formation abilities were characterized by varying concentration of the coexisting oxygen (see Fig. 2-6). The highest ammonia formation property was obtained on the Fe-doped sample. It generated gaseous ammonia even at 10 vol.% of oxygen coexistence. Oxygen coexistence limit for the ammonia formation was 7 vol.% for In-doped catalyst and 3 vol.% for Sc-doped one. Evolution of ammonia

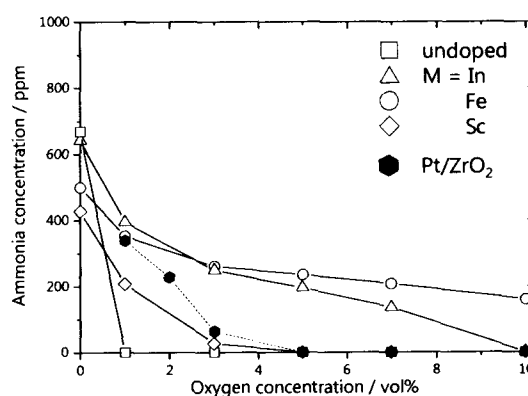


Figure 2-6. Oxygen concentration dependences of ammonia discharge amount from a series of Pt/(Sn_{0.9}M_{0.1})P₂O₇ and Pt/ZrO₂ catalyst from ref. [40] at 140 °C.

gas on the undoped sample was detected only in the oxygen absence condition. It was found that the substituted catalysts have high ammonia formation ability compared with the usual catalysts such as Pt/ZrO₂ which can generate gaseous ammonia in oxygen coexistence less than 5 vol.% [40]. Although the order for the ammonia formation ability (Fe-doped > In-doped > Sc-doped > undoped) does not agree with the deNO_x property, the order for the ammonia product amount in the absence of oxygen is inverse order of the catalytic activity. These results may indicate that the Sc-doped sample immediately adsorb the *in situ* produced ammonia to serve as a reductant for deNO_x reaction, resulting in apparent decrease of ammonia evolution.

In fact, NH₃-TPD measurements support that Sc-doped sample has the most and strongest Brønsted acid sites. Figure 2-7 shows the gas flow rate dependences for NO_x conversion and reductive product selectivity on Fe-doped catalyst (Pt/Sn_{0.9}Fe_{0.1}P₂O₇) at 140 °C. The NO_x conversion decreased at higher gas flow rate because of short contact time between the catalyst and reaction gas, while selectivity for ammonia increased and nitrous oxide (N₂O)

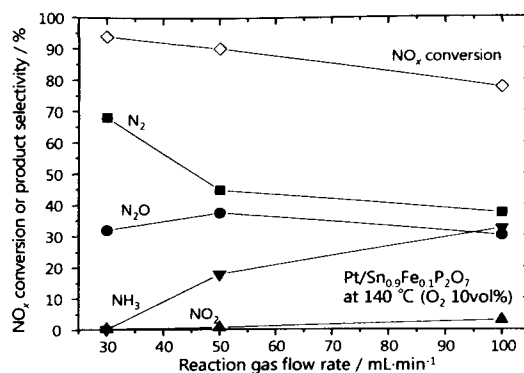


Figure 2-7. Reaction gas flow rate dependences of NO_x conversion (open quary) and selectivity for reductive products, N₂ (filled square), N₂O (filled circle), and NH₃ (filled triangle), on Pt/(Sn_{0.9}Fe_{0.1})P₂O₇ catalyst at 140 °C.

selectivity kept being a constant value. These result suggest that the H₂-SCR proceed in two reaction steps: reduction with hydrogen gives nitrogen, ammonia, and some byproduct of nitrous oxide ($\text{NO}_x + \text{H}_2 \rightarrow \text{N}_2 + \text{NH}_3 + \text{N}_2\text{O} + \text{H}_2\text{O}$), and further NO_x reduction using *in situ* evolved is occurred to form nitrogen ($\text{NO}_x + \text{NH}_3 \rightarrow \text{N}_2 + \text{H}_2\text{O}$). Tronconi et al. have proposed the reaction mechanism of NH₃-SCR in the oxygen coexistence as shown in Fig. 2-8 [41]. According to this mechanism, nitrogen monoxide is once oxidized to NO₂, and then resultant NO₂ is reduced ammonia. Trace amount of NO existence in the unreduced NO_x observed on the substituted catalysts bears out that ammonia intermediate species are once generated by reacting NO_x with hydrogen and then the resultant ammonia reduces NO₂.

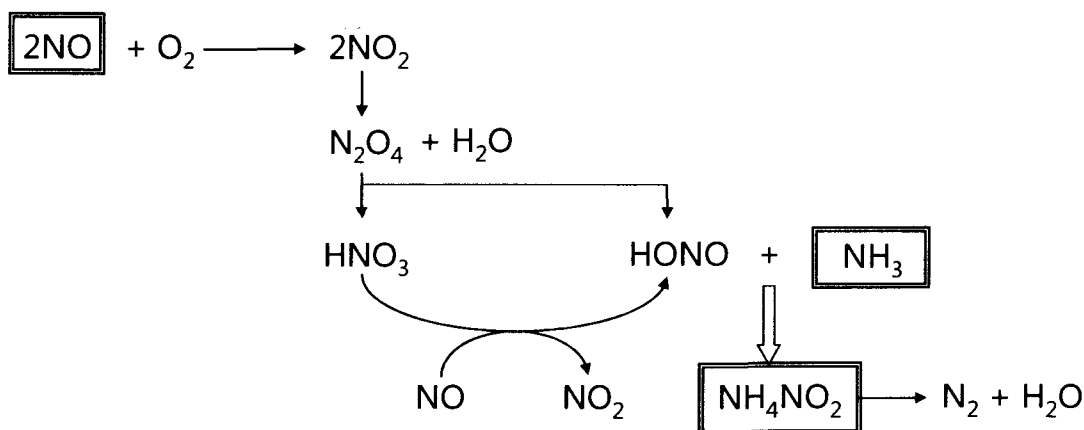
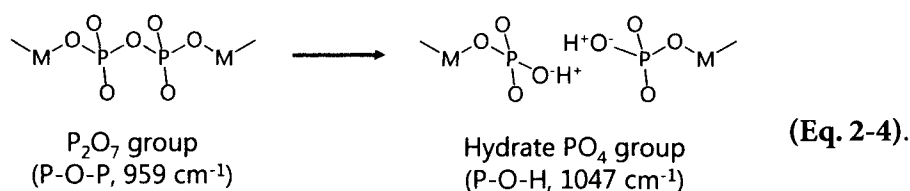


Figure 2-8. The reaction mechanism for NH₃-SCR of NO_x in the presence of oxygen (ref. [41]).

The Brønsted acid sites seem to generate by hydration of oxygen vacancies and/or hydrolysis of pyrophosphate group (P_2O_7). The oxygen vacancies (V_o) formed by substituting trivalent cations for Sn^{4+} sites are hydrated with coexisting water vapor as following reaction [42]:



where V_o , H_i , and O_o^x denote an oxygen vacancy, an incorporated proton, and a lattice oxide ion, respectively. Negative and positive peaks derived from respective $\nu(P-O-P)$ at 959 cm^{-1} and $\nu(P-O-H)$ at 1047 cm^{-1} were observed in the DRIFT spectra (see Fig. 2-4) on a series of $Pt/(Sn,M)P_2O_7$ catalysts [43]. This spectrum suggests that a pyrophosphate unit was hydrolyzed by water generated during the reaction and two protonated orthophosphate units were formed as represented by



The adsorbed NO_x can be protonated by these Brønsted acid site and reduced by the dissociate hydrogen over the platinum. Further studies in needed to elucidate the detail mechanism for ammonia evolution.

2.4. Conclusion

The platinum catalysts loaded on trivalent cations doped tin pyrophosphates, $(Sn,M)P_2O_7$ ($M = In, Fe, \text{ or } Sc$) powders, showed an excellent $deNO_x$ property with high N_2 selectivity even at excess oxygen coexistence (ca. 10 vol.%). Especially, the Sc -doped catalyst achieved more than 90% NO_x conversion with 80% N_2 selectivity. This catalytic property should owe to *in situ* ammonia formation. The platinum catalysts loaded on the above support materials effectively reduced NO_x to ammonia by hydrogen. The *in situ* formed ammonia are immediately adsorbed on the acid sites and served as an additional reductant for NO_x

reduction in the N_2O -free pathway. Such Brønsted acid sites should be evolved by two mechanisms: the hydration of oxygen vacancies and the hydrolysis of pyrophosphate group (P_2O_7).

Hydrogen SCR Reaction over Platinum Catalysts Loaded on Sulfated Metal Oxides

3.1. Introduction

In the last chapter, the hydrogen SCR involving an *in situ* ammonia intermediate formation and following NH_3 -SCR allowed us to obtain the high NO_x conversion with low N_2O emission over a platinum catalyst supported on partially substituted tin pyrophosphates. Ammonia formation and good deNO_x activity are ascribable to the Brønsted acid sites of supporting materials. Surface modifications for metal oxides with acidic molecular groups such as SO_4 , WO_3 , and MoO_3 can create strong solid acid sites. Among them, the sulfated metal oxides are noteworthy as the catalysts or supported materials with their strong acidity. For example, the sulfated zirconia ($H_o < -16.04$) catalyzes the isomerization of *n*-butane to *i*-butane even at room temperature [44]. In addition, they have good tolerance to the SO_x (sulfur oxides) impurity contained in the real exhaust gases [30].

In this chapter, H_2 -SCR characteristics for NO_x over platinum catalyst supported on the sulfated metal oxides powders were studied from the viewpoints of their surface acidity and reaction intermediate. Furthermore, the reaction intermediates were characterized by *in situ* DRIFTS measurements to understand the reaction mechanism.

3.2. Experimental details

Preparation and characterization of platinum catalysts

Sulfated metal oxide powders (denoted as s- MO_x ; $M = \text{Zr, Ce, Al, Ti, Si, and Sn}$) were prepared from the corresponding commercially available metal oxide powders and reagent grade ammonium sulfate. The chemicals were weighed with an atomic ratio of $M:S = 3:1$ and

well mixed in an agate mortar. After drying at 120 °C for 24 h, the mixtures were calcined at 600-800 °C for 3 h in air. Some sulfated samples were also prepared by impregnating the corresponding amorphous metal hydroxides in dilute sulfuric acid solution or sulfuryl chloride, and then they were heated at proper temperature for 3 h according to the previous reported method [45]. Then 1wt% of platinum were loaded by successive impregnation using a $\text{Pt}(\text{NO}_2)_2(\text{NH}_3)_2$ solution. The resultant powders were dried at 120 °C overnight and calcined at 600 °C for 2 h in air. Conventional platinum catalysts supported on pure metal oxides, without sulfating treatment, were also prepared by the same procedure as references.

Catalytic properties for H_2 -SCR of NO_x reduction and reaction intermediates were characterized by a similar manner as described in chapter 2. In addition, thermal analyses, thermogravimetric analysis and differential thermal analysis, were performed using TGA-50 and DTA-50 (Shimadzu). IR spectra were recorded on a Fourier transform infrared spectrometer (FT/IR-430, Jasco) by a KBr method using unsulfated metal oxides as background samples.

3.3. Results and discussion

3.3.1. Pt/s- ZrO_2 catalysts

From the FT-IR spectrum, the peak assigned to $\nu(\text{S-O-S})$ was observed at 1388 cm^{-1} as shown in Fig. 3-1. Also three peaks observed at 1224 , 1144 , and 1056 cm^{-1} are responsible for $\nu(\text{S-O})$. These results indicate that surface of the zirconia was covered by sulfate groups [46]. No peaks derived from a law material (ammonium sulfate) were detected. The specific BET areas of sulfated- and untreated-zirconia powders were

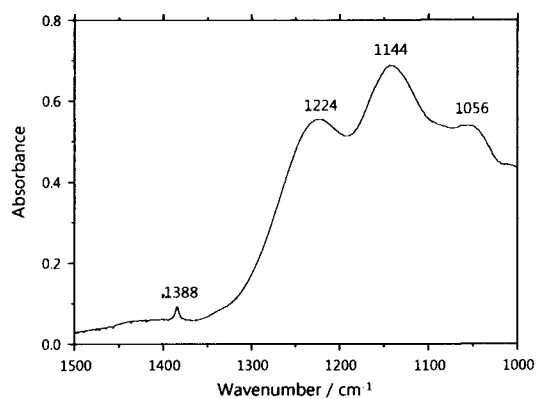


Figure 3-1. An IR spectrum of the sulfated zirconia caicined at 700 °C, KBr method (ZrO_2 powder was as background), scanning time; 50 times, resolution; 4 cm^{-1} .

almost same value about 80-90 $\text{m}^2\cdot\text{g}^{-1}$.

The NO_x conversion and N_2 selectivity of $\text{Pt}/\text{s-ZrO}_2(x)$ (x represents the heating temperature for sulfating treatment) and Pt/ZrO_2 are shown in Fig. 3-2. The $\text{Pt}/\text{s-ZrO}_2(700)$ exhibited the highest NO_x conversion (80%) with 66% N_2 selectivity at 100 $^\circ\text{C}$. This catalytic activity was maintained almost constantly at least for 8 h, and no gaseous ammonia was also detected in the present catalysis system. The higher conversion and selectivity compared to the previously reported values on Pt/ZrO_2 (NO_x conversion: 72%, N_2 selectivity: 57% at 110 $^\circ\text{C}$ [47]) were attained even at lower temperature (100 $^\circ\text{C}$). Although the NO_x conversion decreased over 140 $^\circ\text{C}$, the N_2 selectivity was enhanced up to almost 100% with increasing reaction temperature. In the case of $\text{Pt}/\text{s-ZrO}_2$, the resultant NO_x consisted of mainly NO at lower temperature (< 140 $^\circ\text{C}$), while the $\text{NO}:\text{NO}_2$ ratio in residual NO_x were almost constant value on Pt/ZrO_2 catalyst over the whole temperature range. It implies that NO_x are also mainly reduced *via* NH_3 -SCR scheme, which similar to the reduction mechanism described in chapter 2.. $\text{Pt}/\text{s-ZrO}_2(800)$ catalyst provided somewhat low N_2 selectivity compared with that of $\text{Pt}/\text{s-ZrO}_2(700)$, and non-modified Pt/ZrO_2 showed poor NO_x reducing characteristics at 100 $^\circ\text{C}$ and N_2 selectivity hardly exceeded 60% even at its suitable temperature region. The

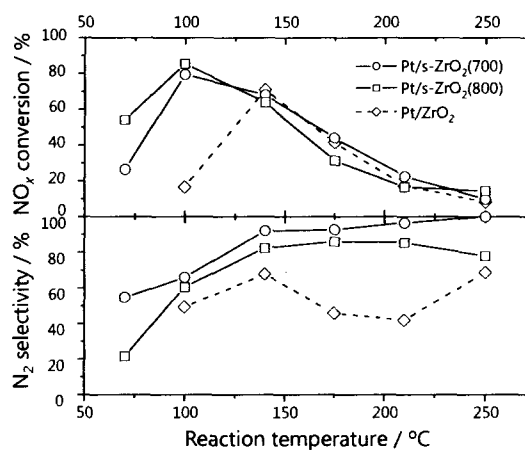


Figure 3-2. Temperature dependences of NO_x conversion and N_2 selectivity on platinum catalysts loaded on sulfated-zirconia calcined at 700 $^\circ\text{C}$ (open circle) and 800 $^\circ\text{C}$ (open square) and Pt/ZrO_2 as a comparison. Weight of catalysts; 0.1g, gas flow rate; 30 $\text{mL}\cdot\text{min}^{-1}$, gas composition; 0.1 vol.% NO , 0.4 vol.% H_2 , 10 vol.% O_2 , and balance of N_2 .

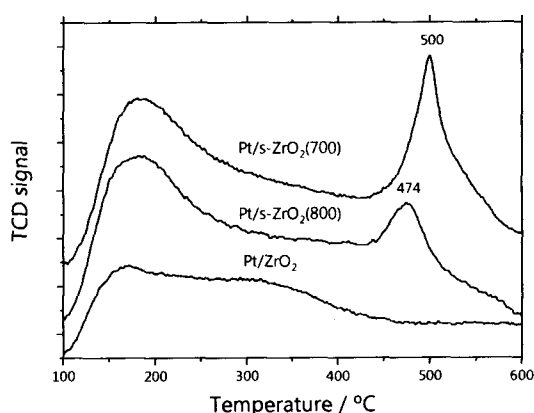


Figure 3-3. NH_3 -TPD profiles of platinum loaded catalysts on s-ZrO_2 and ZrO_2 .

peaks of NH_3 -TPD were observed at 165 °C on Pt/ZrO_2 , 190 and 500 °C on $\text{Pt}/\text{s-ZrO}_2(700)$, and 185 and 475 °C on $\text{Pt}/\text{s-ZrO}_2(800)$. The lower temperature peaks at 160-180 °C correspond to desorption from zirconia surface and those at 475-500 °C were ascribable to the elimination from sulfate groups [48]. The thermoanalyses indicates that ammonium sulfate decomposes at about 410 °C and the fixation of sulfate group on the oxide surface is completed about at 600 °C with the vaporization of extra sulfates as shown in Fig. 3-4. Two DTA peaks at 316 and 410 °C are attributed to the stepwise decomposition ammonium sulfate. The dull decrease of weight observed above 600 °C is attributed to the volatilization of the fixed sulfate groups, where fixed sulfate group desorbed from the surface in order of increasing bond strength. These results suggest that catalytic performance is enhanced by the acid sites of support materials. Un-functionalized zirconia has no strong acid site and resultant Pt/ZrO_2 showed less catalytic activity for H_2 -SCR of NO_x than $\text{Pt}/\text{s-ZrO}_2$ catalysts. In addition, some portion of fixed sulfate group were vaporized during high temperature heating for sulfating treatment and their acid sites were decreased and weakened, resulting in derogation of the de NO_x catalytic activity, as seen in $\text{Pt}/\text{s-ZrO}_2(800)$ catalyst.

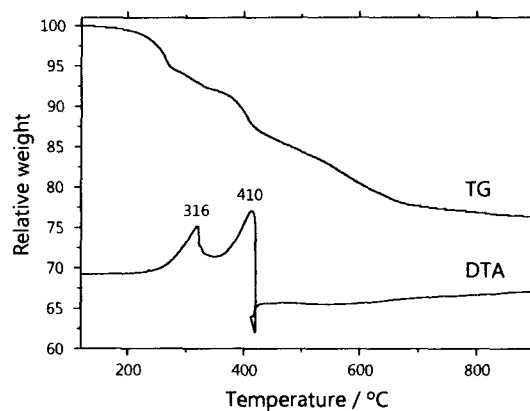


Figure 3-4. TG and DTA profiles for a mixture of ZrO_2 and $(\text{NH}_4)_2\text{SO}_4$ powders.

The ammonium species (3225 , 3047 , 2840 , and 1430 cm^{-1}), cis-HNO_2 (1685 cm^{-1}) and NO_2^- (1260 cm^{-1}) groups [49] were detected by *in situ* DRIFTS measurements on the $\text{Pt}/\text{s-ZrO}_2(700)$ catalyst after feeding reaction gas ($\text{NO} + \text{O}_2 + \text{H}_2$) as shown in Fig. 3-5a. A negative peak at around 1388 cm^{-1} , which attributed to $\nu(\text{S-O-S})$, was also observed. It means that the bridged S-O-S chemical bond has disappeared by feeding the reaction gas. This change was not seen in the presence of nitrogen monoxide and oxygen as reaction gas components (Fig. 3-5b and 3-5c). On the other hand, signal intensity of $\nu(\text{S-O-S})$ was lowered in the

presence of hydrogen (Fig. 3-5d) and water vapor (Fig. 3-5e). In particular, $\nu(\text{S-O-S})$ signal continuously decreased in the presence of reaction gas (Fig. 3-5a) or water vapor (Fig. 3-5e) and only the initial decline were recorded in the case of a hydrogen stream (Fig. 3-5d). From these results, water should be responsible to promote hydrolysis of S-O-S chemical bond, leading the formation of acid site in the following reaction:

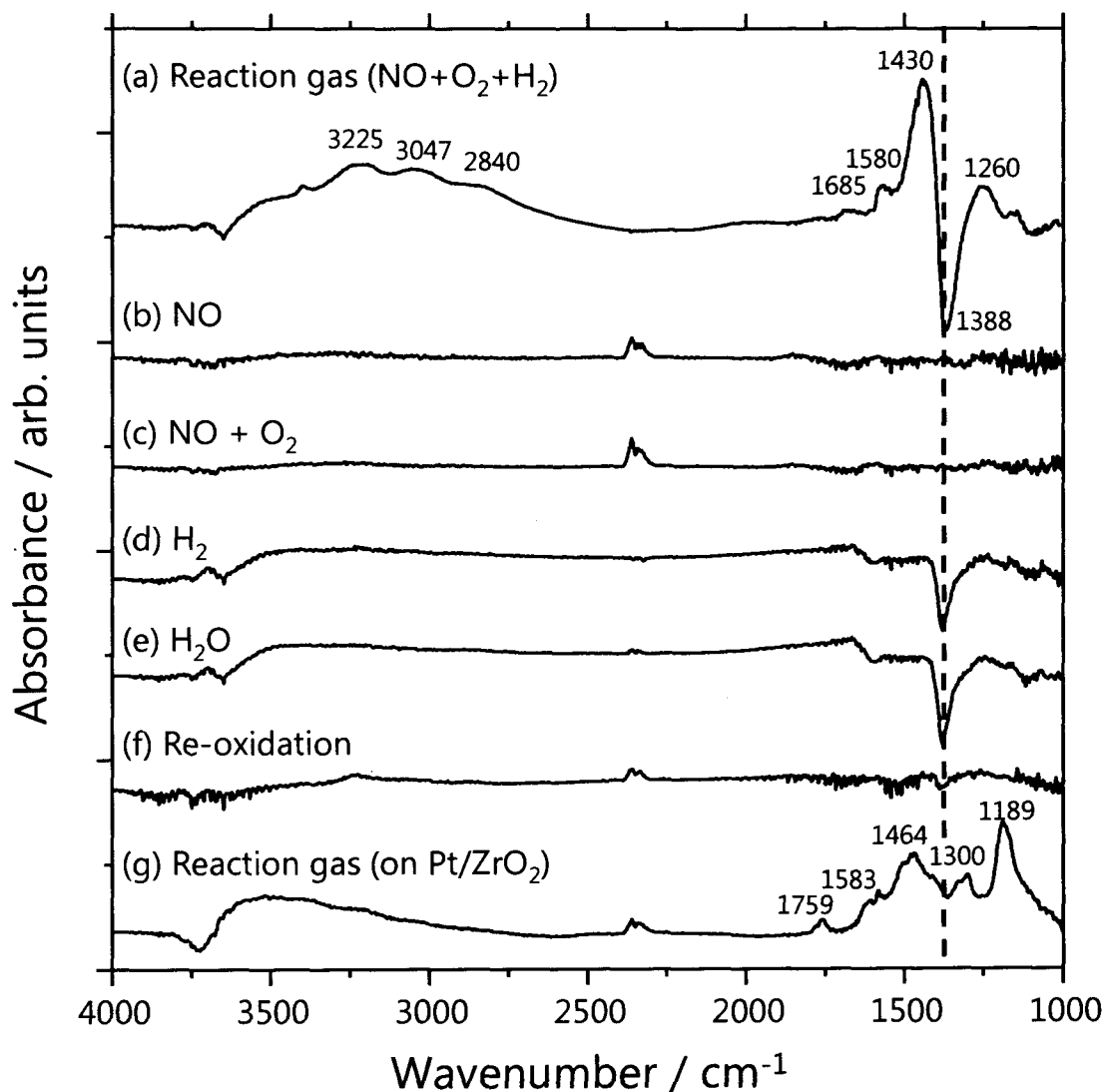
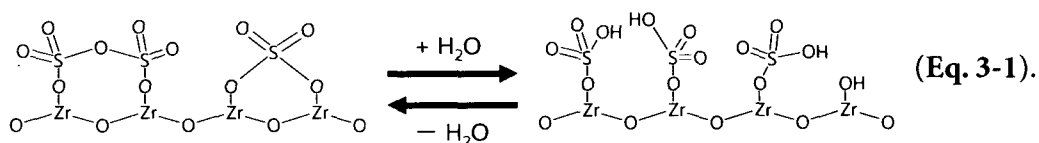


Figure 3-5. *In situ* DRIFT spectra of Pt/s-ZrO₂(700) at 100 °C in flow N₂-based gases: (a) reaction gas (NO + O₂ + H₂), (b) 0.1 vol.% NO, (c) 0.1 vol.% NO and 10 vol.% O₂, (d) 0.4 vol.% H₂, (e) water vapor (about 3 kPa), (f) N₂ after reoxidization at 400 °C and (g) spectra of Pt-ZrO₂ under the same reaction gas as (a). Peaks at around 2400 cm⁻¹ are attributed to CO₂ impurity.

S-O-S or S-O-Zr chemical bonds are transformed to S-OH, in which such Brønsted acid site is known as a superacid. The negative $\nu(\text{S-O-S})$ peak was disappeared by re-oxidizing at 400 °C (Fig. 3-5f). Thus, these results revealed that the acid site formation should be reversible and the fixed sulfate groups hardly vaporize. Nanba et al. have proposed that protons on surface hydroxyl (Zr-OH) groups on Pt/ZrO₂ are responsible for the formation of ammonia intermediates which lead to high NO_x reduction activity [50]. The superacid (S-OH) species can donate protons to adsorbed NO_x species more strongly than Zr-OH group, resulting in the stable fixation of ammonium species even at 100 °C. Such NO_x reduction involving ammonium species may proceed through the same pathway on the non-functionalized Pt/ZrO₂ [51]. On the other hand, the adsorbed intermediates on conventional Pt/ZrO₂ were nitrate groups (NO₃⁻) which are usually observed in H₂-SCR and no ammonium species was detected (Fig. 3-5g).

3.3.2. Pt/s-CeO₂ catalysts

The XRD pattern of the sulfated ceria (s-CeO₂) powder was almost same to the starting ceria powder and they were assigned as fluorite CeO₂ (PDF #34-0394) and any impurity peak such as cerium sulfate was not observed. The s-CeO₂ powders showed three obvious IR bands at 3420, 1630 and 1150 cm⁻¹, and absorption bands derived from ammonium sulfate (3149, 1402, and 1115 cm⁻¹) were not observed in the IR spectra shown in Fig. 3-6. Therefore raw sulfate source should completely decompose on the ceria surface and the sulfate groups were stably fixed onto the surface of ceria.

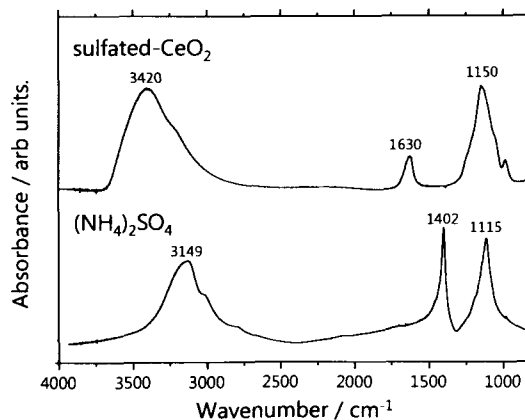


Figure 3-6. An IR spectrum of the sulfated ceria calcined at 700 °C, KBr method (CeO₂ powder was as background), scanning time; 50 times, resolution; 4 cm⁻¹.

Figure 3-7 shows the catalytic performance of Pt/CeO₂ and Pt/s-CeO₂ at a temperature range from 70 to 250 °C. The Pt/CeO₂ catalyst without sulfation treatment showed poor activity through the whole temperatures. Platinum supported catalysts on the basic oxides have been reported to give inferior deNO_x catalytic property compared to those on the acidic oxides [52]. The solid basicity of ceria is responsible to this low catalytic

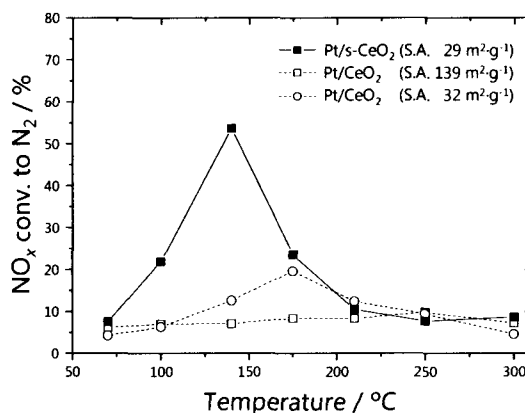


Figure 3-7. Temperature dependences of NO_x conversion and N₂ selectivity on platinum catalysts loaded on CeO₂ and s-CeO₂ powders. Weight of catalysts; 0.1 g, gas flow rate; 30 mL·min⁻¹. The reaction gas; 0.1 vol.% NO, 0.4 vol.% H₂, 10 vol.% O₂, and balance of N₂.

performance. While Pt/s-CeO₂ catalyst showed 87% of NO_x conversion with 65% of N₂ selectivity at 100 °C (conversion to N₂ was 57%), which are superior to the result over platinum catalysts on pure oxides (e.g., Pt/ZrO₂: NO_x conversion, 72%; N₂ selectivity, 57% at 110 °C [47]). NO_x conversion value, however, was sharply decreased at above 175 °C. It is due to the undesirable oxidation of hydrogen by the coexisting oxygen. The respective BET surface area of Pt/CeO₂ and Pt/s-CeO₂ catalysts are 139 and 29 m²·g⁻¹. Despite almost same thermal history, Pt/s-CeO₂ catalyst has significantly low surface area compared with Pt/CeO₂ catalyst. Ammonium sulfate, raw material for sulfate group, seems to be responsible for this decrease. It has melted during the heating for the sulfation treatment at 600 °C, and the molten one acted as not only a sulfating agent but also a flux to promote particle aggregation of ceria particle causing the notable decrease of BET surface area. So that platinum particle loaded on the sulfated-ceria must be enlarged than that on the unsulfated-one. Although we have already reported platinum particle size affects their catalytic property for NO_x reduction, Pt/CeO₂ catalyst prepared from another ceria powder having the almost same surface area value (32 m²·g⁻¹) with the above discussed sulfated-ceria (29 m²·g⁻¹) showed a inferior catalytic performance peaking at 175 °C. It suggests that features of supporting material, such as solid acidity, are major factor rather than the Pt particle size for the present catalysts.

In situ DRIFT spectra of platinum catalysts loaded on sulfated- and pure-ceria are shown in Fig. 3-8. Three broad bands assigned to adsorbed ammonia (or ammonium ions) around 2700-3300 cm^{-1} were only observed in the absence of oxygen on Pt/CeO₂ catalyst. On the other hand, ammonium adsorbate could be observed on Pt/s-CeO₂ catalyst even under the oxygen coexistence condition. These results provide an idea that the surface of sulfated ceria has low affinity against oxygen to enhance the ammonia formation by reacting with H₂ and NO_x. Figure 3-9 shows the O₂-TPD profiles obtained on Pt/s-CeO₂ and Pt/CeO₂ catalysts. Desorption of oxygen from Pt/s-CeO₂ and Pt/CeO₂ catalysts started at 100 and 310 °C, respectively. This result is good accordance with the above idea for decreasing oxygen affinity on Pt/s-CeO₂. As a result, the surface of sulfated catalysts made oxygen poor condition which was preferable to the formation of ammonium intermediate.

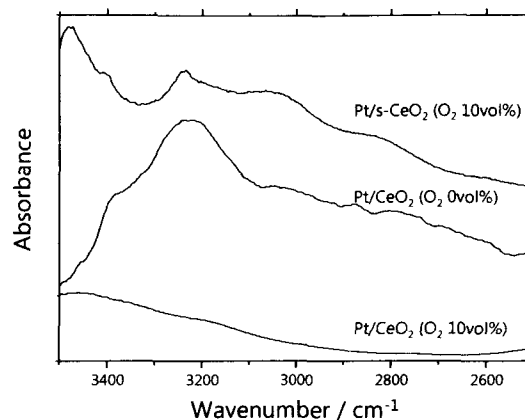


Figure 3-8. *In situ* DRIFT spectra of Pt/CeO₂ and Pt/s-CeO₂ catalysts at 100 °C in N₂ based-gas flow containing NO, H₂ and 10 vol.% of oxygen coexistence and absence.

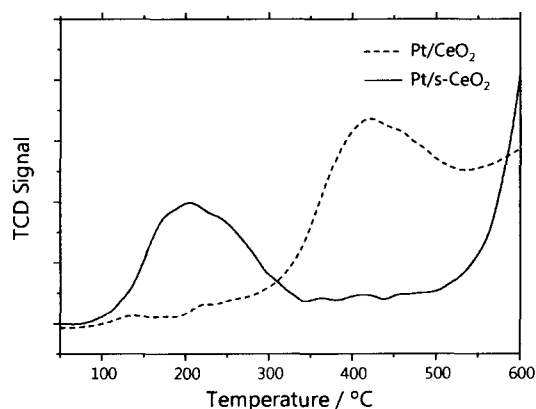


Figure 3-8. Oxygen temperature programmed desorption profiles on Pt/CeO₂ (dashed line) and Pt/s-CeO₂ (solid line) catalysts.

3.3.3. Pt/s-MO_x catalysts (M = Al, Ti, Si, and Sn)

The other metal oxides such as Al₂O₃, TiO₂, and SnO₂ were also sulfated and used as supporting materials for platinum catalysts. All the catalysts were confirmed to be successfully sulfated by checking their infrared spectra. In the case of Al₂O₃ (Fig. 3-10), the sulfation treatment enhanced the catalytic activity for H₂-SCR of NO_x. In particular, it enabled to

reduce about 90% of NO_x with 60% N₂ selectivity at 100 °C, which was better activity than that observed on the un-sulfated Pt/Al₂O₃. Although NO_x conversion values at above 140 °C were almost same to the un-sulfated one, the N₂ selectivity was improved by the sulfating treatment.

On the other hands, platinum catalysts loaded on sulfated-TiO₂, -SiO₂, and -SnO₂ showed almost same catalytic properties compared to with untreated catalysts (Fig. 3-11, 12). The behaviour such as low N₂ selectivity and optimal reduction temperature around 100 °C suggest that NO_x are reduced *via* only conventional H₂-SCR scheme.

In fact, their DRIFT spectra revealed that ammonia intermediate has not incorporated over these catalysts.

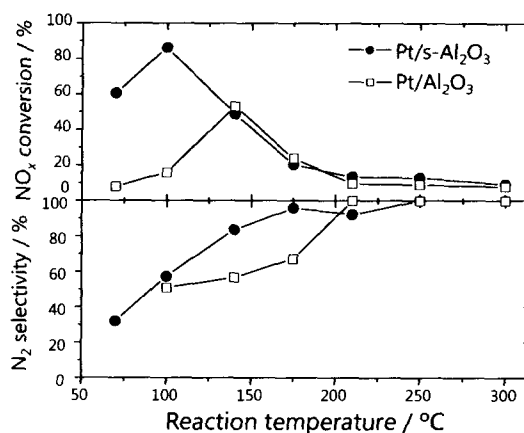


Figure 3-10. Temperature dependences of NO_x conversion and N₂ selectivity on platinum catalysts loaded on Al₂O₃ and s-Al₂O₃ powders. Reaction condition is described above.

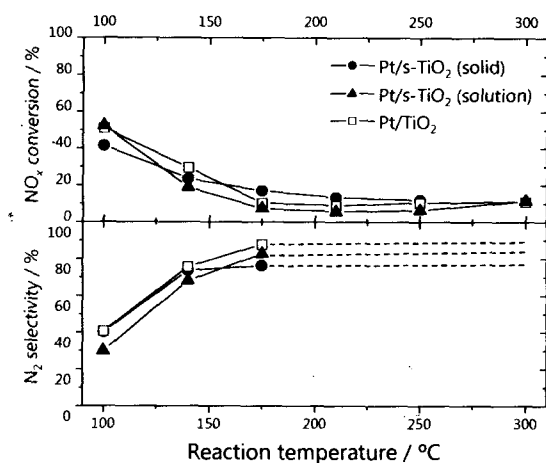


Figure 3-11. Temperature dependences of NO_x conversion and N₂ selectivity on platinum catalysts loaded on TiO₂ (open square) and s-TiO₂ powders prepared by solid-phase sintering (filled circle) or impregnation with sulfuric acid and following calcination (filled triangle). Reaction condition is described above.

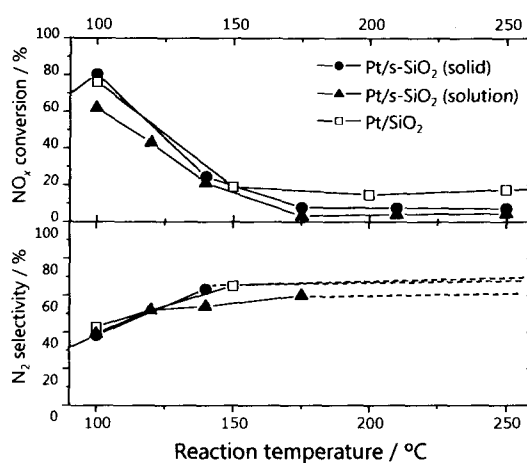


Figure 3-12. Temperature dependences of NO_x conversion and N₂ selectivity on platinum catalysts loaded on SiO₂ (open square) and s-SiO₂ powders prepared by solid-phase sintering (filled circle) or impregnation with sulfuryl chloride and following calcination (filled triangle). Reaction condition is described above.

The electronegativity values of these metal oxides are summarized in Fig. 3-13 using a

following equation:

$$\chi_{\text{oxide}} = \sqrt{x+y} [\chi_M]^x [\chi_O]^y \quad (\text{Eq. 3-2})$$

where χ_{oxide} , χ_M , and χ_O represent electronegativity of gross metal oxide, constructing metal element, and oxygen, respectively. ZrO_2 , CeO_2 , and Al_2O_3 which have lower electronegativity values are known as basic or neutral oxides, while TiO_2 , SiO_2 , and SnO_2 with high electronegativity values are acidic oxides. The acidity-basicity of mother metal oxides may contribute the enhancement in catalytic properties by sulfation treatments. Metal cations of acidic oxides strongly withdraw electron and weaken the polarization between M-O bonds decreasing positive charge of neighboring sulfur atom. As a result of weak polarization, the acidity for fixed sulfate group may be decreased.

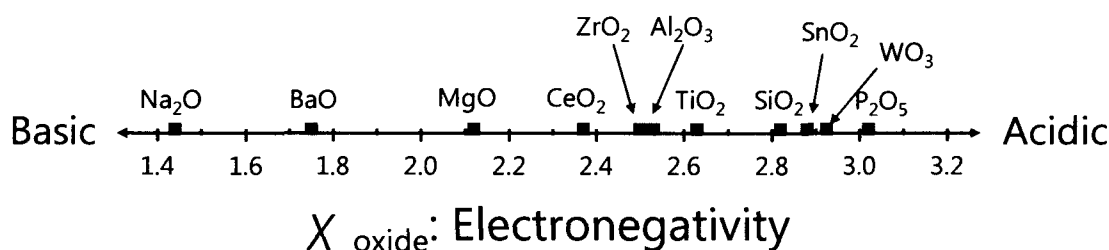


Figure 3-13. Electronegativity values of various metal oxides.

3.4. Conclusion

The sulfation treatment on metal oxide support materials such as ZrO_2 , CeO_2 , and Al_2O_3 remarkably enhances catalytic properties for deNO_x on platinum impregnated catalysts. Because of their low affinity against oxygen adsorption, the catalyst surface is kept as partially oxygen poor condition even in the presence of excess oxygen (10 vol.%). Ammonia intermediate species readily generated by reacting NO_x with hydrogen under these oxygen poor conditions, and worked as a reductant for the following NH₃-SCR reaction with low N₂O yielding. The *in situ* evolved ammonia species were immediately adsorbed onto strong Brønsted acid sites generated by hydrolysis of the bridged -S-O-S- groups on the surface. The high N₂ selectivity is achieved through the reaction between ammonium species and adsorbed

NO_3^- groups through the NH_3 -SCR route. On the other hand, the sulfation treatments for acidic metal oxides could not improve their catalytic activity for NO_x reduction. This result implies that an interaction between mother metal oxides and sulfate groups is responsible to the catalytic property.

Summary

In this thesis, the present author focused two reactions: direct ammonia synthesis by using ruthenium catalysts over Ag-Pd membrane reactors (**Chapter 1**) from hydrogen and nitrogen to use as a reductant for NH_3 -SCR reaction of NO_x , and H_2 -SCR of NO_x involving ammonia formation as an intermediate species on the platinum catalysts supported on metal oxides having solid acidity (**Chapters 2 and 3**).

In Chapter 1, on the Ag-Pd hydrogen permeable membrane reactor, ammonia formation properties of ruthenium catalysts are considerably enhanced by supplying the highly reactive atomic hydrogen. Hydrogen poisoning for ruthenium catalysts are effectively suppressed by supplying hydrogen through the hydrogen penetrative membrane. The gaseous type membrane reactor gives about 1.5-2 times of ammonia formation activity as much as the conventional flow type reaction even at high-pressure condition (0.6 MPa) due to the above suppression effect for hydrogen poisoning. The water electrolysis type membrane reactor produces ammonia even at low temperature about 100 °C. The electrodeposited ruthenium metal catalysts have porous structure formed by template effect of co-deposited zinc component and they are activated by electron donation from the Ag-Pd anode. Although their catalytic activity immediately decreases by sintering with ammonia formation heat, it is effectively improved by coating with a thin alumina layer worked as a buffer one.

In Chapter 2, $\text{Pt}/(\text{Sn},\text{M})\text{P}_2\text{O}_7$ ($\text{M} = \text{In}, \text{Fe}, \text{or Sc}$) catalysts provide excellent de NO_x properties with high N_2 selectivity even at 10 vol.% of oxygen concentration. Especially, the Sc-doped catalyst achieves more than 90% NO_x conversion with 80% N_2 selectivity. The reduction of NO_x over these catalysts proceeds in two steps: the H_2 -SCR generating N_2 , NH_3 , H_2O , and N_2O as a by-product, and the subsequent NH_3 -SCR utilizing above evolved ammonia intermediate with little N_2O emission. Reactivity and formation ability of the ammonia intermediates are depend on their Brønsted acid sites evolved by two mechanisms. One is the hydration of oxygen vacancies and another is the hydrolysis of pyrophosphate group (P_2O_7).

Such acid sites adsorb the ammonia intermediate to be used for the following NH_3 -SCR of NO_x with high N_2 yield.

In Chapter 3, Brønsted acid sites are produced by a sulfation treatment for various metal oxides. DeNO_x catalytic activity of platinum catalysts loaded on ZrO_2 , CeO_2 , and Al_2O_3 support materials remarkably enhanced by the sulfating their surface. The reason of these improvements owes to their low affinity against oxygen adsorption. As a result, partially oxygen-poor atmosphere which favored to ammonia formation is formed on the surface of catalysts. Ammonia intermediate species readily generates by reacting NO_x with hydrogen under these oxygen poor conditions, and acts as a reductant for the following NH_3 -SCR reaction with low N_2O evolution. Since the sulfation treatment can not enhance catalytic performance in the case of acidic oxide supports. This solid acidity seems to prevent sulfating groups from expression of Brønsted acidity.

References and Notes

- [1] B. Metz, O. R. Davidson, P. Bosch, R. Dave, L. Meyer, *Contribution of Working group III to the Fourth Assessment Report of the Intergovernmental Panel in Climate Change*, Cambridge University Press, Cambridge, United Kingdom, <http://www.mnp.nl/ipcc/pages_media/ar4.html>, **2007**.
- [2] C. Erdmenger, H. Lehmann, K. Muschen, J. Tambke, S. Mayr, and K. Kuhnhenh, *Energ. Pol.* **2009**, *37*, 158.
- [3] *National Greenhouse Gas Inventory Report of JAPAN*, ed. by Greenhouse Gas Inventory Office of Japan, National Institute for Environmental Studies, Japan, <http://www-gio.nies.go.jp/aboutghg/nir/2008/NIR_JPN_2008_v4.0_E.pdf>, **2008**.
- [4] K. Hirata, *Shokubai* (in Japanese) **2006**, *48*, 593.
- [5] N. Masaki, K. Hirata, H. Akagawa, *Jidosha Gijutsu* (in Japanese) **2005**, *59*, 128.
- [6] K. Hirata, N. Masaki, H. Akagawa, *Jidosha Gijutsu* (in Japanese) **2006**, *60*, 28.
- [7] N. Miyoshi, S. Matsumoto, K. Katoh, T. Tanaka, J. Harada, N. Takahashi, K. Yokota, M. Sugiura, K. Kasahara, *SAE Tech. Paper* **1995**, 95-0809.
- [8] N. Takahashi, H. Shinjoh, T. Iijima, T. Suzuki, K. Yamazaki, K. Yokota, H. Suzuki, N. Miyoshi, S. Matsumoto, T. Tanizawa, T. Tanaka, S. Tateishi, K. Kasahara, *Catal. Today* **1996**, *27*, 63.
- [9] M. Takeuchi, S. Matsumoto, *Topics Catal.* **2004**, *28*, 151.
- [10] S. Matsumoto, *Catal. Today* **2004**, *90*, 183.
- [11] N. Fritz, W. Mathes, J. Zürbig, R. Mueller, *SAE Tech. Paper* **1999**, 01-0111.
- [12] S. R. Tennison, *Catalytic Ammonia Synthesis*, ed. by J. R. Jennings, Plenum, New York, **1991**, p. 303.
- [13] K. Aika, A. Ohya, A. Ozaki, Y. Inoue, I. Yasumori, *J. Catal.* **1985**, *92*, 305.
- [14] K. Aika, T. Takano, S. Murata, *J. Catal.* **1992**, *136*, 126.
- [15] M. Nagao, T. Kamiya, P. Heo, A. Tomita, T. Hibino, M. Sano, *J. Electrochem. Soc.* **2006**,

153, A1604.

- [16] A. Tomita, T. Yoshii, S. Teranishi, M. Nagao, T. Hibino, *J. Catal.* **2007**, *247*, 137.
- [17] J. G. Speight, *Lange's Handbook of Chemistry 16th ed.*, McGraw-Hill, New York, **2005**, p. 1.160.
- [18] (a) K. Aika, M. Kumasaka, T. Oma, O. Kato, H. Matsuda, N. Watanabe, K. Yamazaki, A. Ozaki, T. Onishi, *Appl. Catal.* **1986**, *28*, 57; (b) F. Rosowski, A. Hornung, O. Hinrichsen, D. Herein, M. Muhler, G. Ertl, *Appl. Catal. A* **1997**, *151*, 443; (c) F. Rosowski, A. Hornung, O. Hinrichsen, D. Herein, *Angew. Chem. Int. Ed.* **2001**, *40*, 1061; (d) P. Moggi, G. Predieri, A. Maione, *Catal. Lett.* **2002**, *79*, 7; (e) B. Fastrup, *Catal. Lett.* **1997**, *48*, 111; (f) S. E. Siporin, B. C. McClaine, S. L. Anderson, R. J. Davis, *Catal. Lett.* **2002**, *81*, 265; (g) Z. Kowalczyk, M. Krukowski, W. Raróg-Pilecka, D. Szmigiel, J. Zielinski, *Appl. Catal. A* **2003**, *248*, 67; (h) H. S. Zeng, K. Inazu, K. Aika, *J. Catal.* **2002**, *211* 33; (i) Z. H. Zhong, K. Aika, *J. Catal.* **1998**, *173*, 535.
- [19] M. Itoh, K. Machida, G. Adachi, *Chem. Lett.* **2000**, 1162.
- [20] The Committee of Reference Catalysis, Catalysis Society of Japan, *Shokubai* (in Japanese) **1986**, *28*, 41.
- [21] R. A. D-Betta, *J. Catal.* **1974**, *34*, 57.
- [22] D. Dollimore, G. R. Heal, *J. Colloid Interf. Sci.* **1970**, *33*, 508.
- [23] A. D'Orenelas, A. Theolier, A. Choplin, J. M. Basset, *Inorg. Chem.* **1988**, *27*, 1261.
- [24] R. S. Roth, T. Nagas, L. P. Cook, *Phase Diagrams for Ceramists volume IV*, American Ceramics Society, **1981**, Figure 5418.
- [25] A. Trovarelli, G. Dolcetti, C. Leitenburg, J. Kašpar, P. Finetti, A. Santoni, *J. Chem. Soc. Faraday Trans.* **1992**, *88*, 1311.
- [26] R. N. Blumenthal, R. L. Hofmaier, *J. Electrochem. Soc.* **1974**, *121*, 126.
- [27] Y. Niwa, K. Aika, *J. Catal.* **1996**, *162*, 138.
- [28] C. Vayenas, S. Brosda, *Solid State Ionics* **2002**, *154/155*, 243.
- [29] M. Iwamoto, H. Yahiro, Y. Yu-u, S. Shundo, N. Mizuno, *Shokubai* (in Japanese) **1990**, *32*,

- [30] H. Ohtsuka, T. Tabata, *Appl. Catal. B* **2001**, *29*, 177.
- [31] N. Macleod, R. M. Lambert, *Appl. Catal. B* **2002**, *35*, 269.
- [32] M. Markvart, Vl. Pour, *J. Catal.* **1967**, *7*, 279.
- [33] M. Koebel, M. Elsener, T. Marti, *Combust. Sci. Tech.* **1996**, *121*, 85.
- [34] S. Roy, B. Viswanath, M. S. Hegde, G. Madras, *J. Phys. Chem. C* **2008**, *112*, 6002.
- [35] M. Iwamoto, M. Furukawa, S. Kagawa, *Stud. Surf. Sci. Catal.* **1986**, *28*, 943.
- [36] N. Imanaka, T. Masui, H. Masaki, *Adv. Mater.* **2007**, *19*, 3660.
- [37] T. Nanba, C. Kohno, S. Masukawa, J. Uchisawa, N. Nakayama, A. Obuchi, *Appl. Catal. B* **2003**, *46*, 353.
- [38] J. Shibata, M. Hashimoto, K. Shimizu, H. Yoshida, T. Hattori, A. Satsuma, *J. Phys. Chem. B* **2004**, *108*, 18327.
- [39] R. D. Shannon, *Acta Crystallogr. Sect. A* **1976**, *32*, 751.
- [40] T. Nanba, C. Kohno, S. Masukawa, J. Uchisawa, N. Nakayama, A. Obuchi, *Appl. Catal. B* **2003**, *46*, 353.
- [41] C. Ciardelli, I. Nova, E. Tronconi, D. Chatterjee, B. B-Konrad, M. Weibel, B. Krutzsch, *Appl. Catal. B* **2007**, *70*, 80.
- [42] A. Tomita, N. Kajiyama, T. Kamiya, M. Nagao, T. Hibino, *J. Electrochem. Soc.* **2007**, *154*, B1265.
- [43] R. M. Silverstein, F. X. Webster, *Spectrometric Identification of Organic Compounds Sixth Edition*, John Wiley, New York, **1998**, Chapter 3.
- [44] K. Arata, M. Hino, *Mater. Chem. Phys.* **1990**, *26*, 213.
- [45] K. Arata, M. Hino, *Hyomen* (in Japanese) **1981**, *19*, 75; M. Hino, K. Arata, *Hyomen* (in Japanese) **1990**, *28*, 481.
- [46] M. Bensitel, O. Saur, J.-C. Lavalley, B. A. Morrow, *Mater. Chem. Phys.* **1988**, *19*, 147.
- [47] M. Machida, T. Watanabe, S. Ikeda, T. Kijima, *Catal. Commun.* **2002**, *3*, 233.
- [48] A. Corma, V. Fornés, M. I. J-Rajadell, J. M. L. Nieto, *Appl. Catal. A* **1994**, *116*, 151.

- [49] M. Kantcheva, E. Z. Ciftlikli, *J. Phys. Chem. B* **2002**, *106*, 3941.
- [50] T. Nanba, F. Meunier, C. Hardacre, J. P. Breen, R. Burch, S. Masukawa, J. Uchisawa, A. Obuchi, *100th Catalysis Society of Japan Meeting Abstracts (Shokubai)*, **2007**, *49*, 518.
- [51] T. Nanba, K. Sugawara, S. Masukawa, J. Uchisawa, A. Obuchi, *Topics Catal.* **2007**, *42-43*, 129.
- [52] M. Machida, S. Ikeda, D. Kurogi, T. Kijima, *Appl. Catal. B* **2001**, *35*, 107.

List of Publications

Publications

1. Synergistic Effect of MgO and CeO₂ as a Support for Ruthenium Catalysts in Ammonia Synthesis
Makoto Saito, Masahiro Itoh, Jun Iwamoto, Cheng-Yu Li, Ken-ichi Machida,
Catalysis Letters, **2006**, Vol. 106(3-4), pp. 107-110.
2. Effective Suppression of Hydrogen Poisoning from a Ru-based Catalyst in a Ag-Pd Membrane Reactor
Makoto Saito, Masahiro Itoh, Jun Iwamoto, Ken-ichi Machida,
Bulletin of the Chemical Society of Japan, **2007**, Vol.80(8), pp. 1630-1634.
3. Low Temperature Hydrogen Selective Catalytic Reduction of NO_x on Pt/sulfated-ZrO₂ Catalysts under Excess Oxygen Conditions
Makoto Saito, Masahiro Itoh, Jun Iwamoto, Ken-ichi Machida,
Chemistry Letters, **2008**, Vol. 37, pp. 1210-1211.
4. Hydrogen Selective Catalytic Reduction of NO_x Assisted by *In situ* Ammonia Formation over Pt Catalyst Supported on Fe-doped Tin Phosphate
Makoto Saito, Masahiro Itoh, Jun Iwamoto, Ken-ichi Machida,
Chemistry Letters, **2008**, Vol. 37, pp. 1226-1227.
5. Hydrogen SCR of NO_x over Metal Oxide Supported Pt Catalysts *via In situ* Ammonium Intermediate Formation and Subsequent Pseudo Ammonia SCR Reaction
Makoto Saito, Masahiro Itoh, Jun Iwamoto, Ken-ichi Machida,
in preparation.

6. Hydrogen SCR for NO_x under Oxygen-rich Conditions over Platinum Catalysts Loaded on Sulfated-ceria Supports with Low Affinity for Oxygen Adsorption

Makoto Saito, Koji Motoki, Masahiro Itoh, Jun Iwamoto, Ken-ichi Machida,
Catalysis Communications, in contribution.

7. Selective NO_x Reduction with Hydrogen under Oxygen-rich Conditions over Platinum Catalysts Loaded on Sulfated-MO_x powders: Relationship between Electronegativity of Metal Oxides and Promotion Effect of Sulfating Treatment for Catalytic Performance

Makoto Saito, Koji Motoki, Masahiro Itoh, Jun Iwamoto, Ken-ichi Machida,
in preparation.

8. Hydrogen SCR Characteristics for NO_x over Pt catalysts supported on Metal Phosphates

Makoto Saito, Masahiko Takehara, Masahiro Itoh, Jun Iwamoto, Ken-ichi Machida,
in preparation.

Supplementary Publications

1. High Dependence for Reaction Pressure on Ru/(MgO-CeO₂)/Ag-Pd Ammonia Synthesis Membrane Reactor
Masahiro Itoh, Makoto Saito, Cheng-Yu Li, Jun Iwamoto, Ken-ichi Machida,
Chemistry Letters, **2005**, Vol. 34(8), pp. 1104-1105.
2. Ammonia Synthesis on Magnesia Supported Ruthenium Catalysts with Mesoporous Structure
Jun Iwamoto, Masahiro Itoh, Yoshio Kajita, Makoto Saito, Ken-ichi Machida,
Catalysis Communications, **2007**, Vol. 8, pp. 941-944.
3. Ammonia Synthesis Using Atomic Hydrogen Supplied from Silver-Palladium Alloy Membrane
Masahiro Itoh, Makoto Saito, Naoki Tajima, Ken-ichi Machida,
Materials Science Forum, **2007**, Vols. 561-565, pp. 1597-1600.
4. Influence of Supported-metal Characteristics on deNO_x Catalytic Activity over Pt/CeO₂
Masahiro Itoh, Makoto Saito, Masahiko Takehara, Koji Motoki, Jun Iwamoto,
Ken-ichi Machida,
Journal of Molecular Catalysis A, to be published.
5. Formation of NaNbO₃-based conductive crystal lines on glass surface by Yb fiber laser irradiation
Maolin Pang, Ryota Suzuki, Makoto Saito, Ken-ichi Machida, Hiromasa Hanzawa,
Yoshihiro Nojiri, Shigeo Tanase,
Journal of Applied Physics, **2008**, Vol. 103(1), pp. 013112/1-013112/4.

6. Fabrication and crystal line patterning of $\text{Li}_{1.3}\text{Al}_{0.3}\text{Ti}_{1.7}(\text{PO}_4)_3$ ion conductive glass by Ni atom heat processing method

Maolin Pang, Ryota Suzuki, Makoto Saito, Ken-ichi Machida, Hiromasa Hanzawa,
Yoshihiro Nojiri, Shigeo Tanase,

Applied Physics Letters, **2008**, Vol. 92(4), pp. 041112/1-041112/3.

7. Crystal Line Patterning and Enhanced Ion Conductivity of $\text{Li}(\text{Ge,Ti})_2(\text{PO}_4)_3$ Glasses by Yb Fiber Laser Irradiation

Maolin Pang, Ryota Suzuki, Makoto Saito, Ken-ichi Machida, Hiromasa Hanzawa,
Yoshihiro Nojiri, Shigeo Tanase,

Journal of the Electrochemical Society, **2008**, Vol. 155(6), pp. P74-P77.

Acknowledgment

I would like to express my profound gratitude to everyone who involved in my studies from April 2003 to March 2009 at Osaka University.

First of all, I would like express my sincerest gratitude to my supervisor Professor Dr. Ken-ichi Machida at the Center for Advanced Science and Innovation, Osaka University, for giving me the opportunity to study about catalysts in his laboratory. I appreciate his fruitful advises and comments, continuous encouragement, and concern throughout the work.

I would also like to be grateful to Professors Dr. Nobuhito Imanaka (Division of Applied Chemistry) and Dr. Hiromi Yamashita (Division of Materials and Manufacturing Science), Graduated School of Engineering, Osaka University, for reviewing this thesis and suggesting valuable comments.

I would like to cordially thank Dr. Masahiro Itoh for his guidance, suggestions, and courteous attention throughout this work. I believe that this thesis was never possible without numerous advices and discussions with him. I would like to be grateful to Mr. Sho-ichi Ichihara for his incredible advices and comments. His every word has grown me from an apprentice to a scientist. I am very glad to dedicate this thesis to him as his pupil. I would like to be obliged to Mr. Jun Iwamoto and his co-workers, Honda R&D Co., Ltd., for their kind measurements and helpful discussions on catalysts.

I would like to express a special thanks to my co-workers, Dr. Cheng-Yu Li, Mr. Naoki Tajima, Mr. Koji Motoki, and Mr. Masahiko Takehara for their helpful assistance, support and daily discussions. This work was hardly achieved without their contribution. I would like to appreciate my present and former colleagues of the research group under the direction of Professor Dr. Ken-ichi Machida for their concern and friendship: Mr. A. Hamaguchi, Dr. D-S. Li, Dr. S. Suzuki, Dr. H. Hanzawa, Dr. T. Horikawa, Dr. J-R. Liu, Dr. X-Q. Piao, Dr. H-L. Liang, Ms. S. Takei, Mr. T. Kawasaki, Dr. K. Miura, Mr. R. Suzuki, Mr. F. Shogano, Dr. S. Hatta, Dr. S. Ishikawa, Dr. G-H. Zhang, Dr. M-L. Pang, Mr. H-C. Zhang, Mr. K. Tanaka, Mr. H-G Liu, Mr. M.

Terada, Mr. M. Nishimoto, Mr. M. Fujitani, Mr. T. Nishikawa, Mr. M. Zou, Mr. K. Iwaya, Mr. A. Tatsumi, and Mr. N. Takemura. I wish Mr. B-G. Yun success in his Ph. D. course in the next years. I would like to thank the secretaries: Ms. M. Okabe and Ms. M. Yagi for their kindness assistance.

I acknowledge the Japan Society for the Promotion of Science (JSPS) for their financial support.

Finally, I would like to express sincere gratitude to my parents: Ms. Yoshie Saito and Mr. Seizo Saito, junior brother Mr. Keiji Saito and my dearest roommates: Ms. Eriko Morikawa and Ms. Misuzu Akiyama for their hearty support, understanding, and encouragement.

It's my great pleasure to finish my Ph. D. work with your incredible support.

Makoto Saito

Suita, Osaka

March 2009

